12-2021

Temperature Effect on the Mechanical Properties of Steel Fiber Reinforced Ultra-High-Performance Concrete

Jenny Bernadette Gomes
Utah State University

Recommended Citation

UtahStateUniversity
MERRILL-CAZIER LIBRARY

TEMPERATURE EFFECT ON THE MECHANICAL PROPERTIES OF STEEL FIBER

REINFORCED ULTRA-HIGH-PERFORMANCE CONCRETE

by

Jenny Bernadette Gomes

A thesis submitted in partial fulfillment
of the requirements for the degree

of

MASTER OF SCIENCE

in

Civil and Environmental Engineering

Approved:

_____   _____
Andrew Sorensen, Ph.D.   Shuna Ni, Ph.D.
Major Professor   Committee Member

_____   _____
John D Rice, Ph.D.   D. Richard Cutler, Ph.D.
Committee Member   Interim Vice Provost
                                          of Graduate Studies

UTAH STATE UNIVERSITY
Logan, Utah

2021

ABSTRACT

Temperature Effect on The Mechanical Properties of Steel Fiber Reinforced Ultra-High-

Performance Concrete

by

Jenny Bernadette Gomes, Master of Science

Utah State University, 2021

Major Professor: Dr. Andrew Sorensen
Department: Civil and Environmental Engineering

In recent years ultra-high-performance concrete (UHPC) has seen a significant improvement in its mechanical properties and an expansion in applications. UHPC is an advantageous material in terms of high strength, ductility, flexural capacity, and toughness. UHPC has been successfully applied in cryogenic, polar region, deep sea, and civil constructions. The addition of steel fiber to the UHPC mix enhances the strength, and flexural toughness in a significant way. Compared to normal Portland cement concrete, fiber reinforced UHPC behaves differently in freezing to elevated temperature because of its structure, curing procedure, cooling rate, freeze-thaw cycle performance, and composite fiber action. Although there has been substantial development in UHPC, still there is a knowledge gap in terms of the compressive strength and flexural toughness under variant temperatures. The objective of this investigation is to evaluate the compressive strength, flexural toughness, and static modulus of elasticity of UHPC under variant temperature as a function of steel fiber percentage.

The study includes 330 steel fiber reinforced UHPC cylinder and beam specimens with different steel fiber percentages involving a special curing system with lime water and

curing at elevated temperature in an oven. The existing literature shows that the strength of UHPC largely depends on the curing atmosphere such as moisture content and temperature in short and long-term gain of strength. The specimens are kept in freeze thaw chamber afterward to attain the target temperatures before the strength, toughness, and dynamic modulus tests have taken place. Although, at present, many scholars have studied the temperature effect on mechanical properties of ordinary and high-performance concrete there is no research found on UHPC exhibiting the effect of ambient temperature on flexural toughness and strength. In addition to the experimental study, the results are compared and evaluated comprehensively, and numerical models are prepared for static modulus of elasticity under the temperature and steel fiber variation from experimental and design value data. The obtained results reveal that temperature effects the mechanical properties significantly at service level and the steel fibers effect indistinctly up to 1.25% fiber volume.

(110 pages)

PUBLIC ABSTRACT

Temperature Effect on The Mechanical Properties of Steel Fiber Reinforced Ultra-High-Performance Concrete

by

Jenny Bernadette Gomes

The contemporary innovation in concrete technology is ultra-high-performance concrete (UHPC). In this work, mechanical properties of UHPC are studied at ambient terrestrial temperature conditions. Specimens are prepared under laboratory environments maintaining the temperature of -25^0C, -5^0C, 15^0C, 35^0C, and 55^0C. A freeze thaw chamber is utilized to condition the specimens at specified temperatures. Compressive strength, flexural strength, toughness, and modulus of elasticity are determined under varying temperature and steel fiber volume content. The results indicate that both temperature and steel fibers have effect on the mechanical properties of UHPC. The flexural and compressive strength show an opposite trend of strength under the temperature variations. Effect on modulus of elasticity is similar to compressive strength. Numerical relations are developed among modulus of elasticity and compressive strength isolating both temperature and steel fiber volume.

ACKNOWLEDGMENTS

CONTENTS

LIST OF TABLES

LIST OF FIGURES

LIST OF SYMBOLS AND NOTATIONS

SF	Steel fiber
MOE	Modulus of elasticity
MOE'	Design value modulus of elasticity
f'_{cf}	Predicted compressive strength
f_{tf}	Predicted tensile strength
f_{rf}	Predicted modulus of rupture
V_f	Steel fiber volume fraction

CHAPTER 1

INTRODUCTION

1.1   General Background and Motivation

Advances in concrete technology have been leading the research to develop high

compressive strength and ductile concretes that eventually led to the development of

ultra-high-performance concrete (UHPC). Initially known as reactive powder concrete

(Richard, 1995), UHPC was first commercially used in Denmark for security purposes

such as vaults and protective defense construction (Schmidt and Fehling 2005). UHPC is

generally defined as a highly compacted cementitious composite with high compressive

strength around 20 ksi, consisting of low water-binder ratio, silica fume content, large

amounts of superplasticizer and no coarse aggregate (Richard, 1995). The fine particles

are enough to fill the interstitial voids that creates a dense concrete matrix to prevent the

micro cracks within the matrix (Yang et al. 2011) facilitating high compressive and

tensile strength, improved toughness and ductility, excellent energy absorption capacity

(Wang and Gao, 2016; Shi et al., 2015), and greater resistance to freeze thaw cycles

(Graybeal and Tanesi, 2008; Alkaysi et al., 2016). The high strength is useful in long

structural members (Rabbat and Russell, 1982) and in thin shell structures for reduction

in section (Graybeal, 2011). Additionally, UHPC has drawn attention for improved blast

and impact resistance to counter terrorist attack (Thomas and Sorensen, 2017; Thomas et

al. 2017).

Concrete is exposed to various ambient temperatures during its service life which

imparts a significant effect on the mechanical properties of concrete. At normal service

level operating ambient temperatures the compressive strength, toughness, and ductility improve greatly with the addition of fibers (Kie and Ju, 2004). However, Dugat and others (1996) found that a fiber dosage rate above 3% decreases the toughness. In below zero temperatures concrete properties are affected due to the formation of microcracks that holds water that eventually freezes resulting in degradation of the properties of concrete significantly for continuous freezing and thawing cycles (Karbhari at el., 2002). Conversely, compressive strength, and elastic modulus are observed to increase in ordinary concrete as a function of decreasing temperature (Krstulovic-Opara, 2007). On the other hand, ordinary and high-performance concrete show a decrease in compressive strength at elevated temperatures (Husem, 2006). However, UHPC may behave in different manner than that of conventional concrete because of its special compacted matrix. As the application of UHPC is growing the need for research on the effect of temperature on UHPC has drawn attention to evaluate the compressive strength and toughness from below zero to raised terrestrial temperature. Up until now, no research is found that studies the behavior of steel fiber reinforced UHPC under terrestrial temperature.

To further the studies on UHPC, a generalized relationship among temperature, steel fiber dosage rate, compressive strength, static modulus of elasticity, and toughness needs to be developed. The relationship would allow researchers and engineering practitioners to better understand the micro level performance and the efficient application of this material in large scale constructions. In order to aid the existing research, this experimental study is designed to investigate the variation in compressive

strength and toughness as a function of temperature and steel fiber dosage rate. Additionally, the static elastic modulus is investigated for the variant steel fiber percentages. The broad impact of this study is to depict a broad picture of the effect from freezing to elevated temperatures on the mechanical properties of UHPC. This is especially important for steel fiber reinforced UHPC as the mechanical properties of steel are much more temperature dependent than those of concrete.

1.2   Problem Statement and Scope

The research presented in this thesis is designed to determine the effect of temperature, from freezing to elevated temperatures, on the mechanical properties of steel fiber reinforced UHPC. Specifically, the compressive strength, flexural capacity, and toughness of steel fiber reinforced UHPC is studied as a function of temperature and fiber dosage rate.

This study answers the following questions in order to provide a better understanding on the behavior of UHPC at different temperatures and at various fiber dosage rates:

1. How does the temperature affect the compressive strength of steel fiber reinforced UHPC? Are the toughness and flexural behavior of steel fiber reinforced UHPC temperature dependent?

2. How do the steel fibers contribute to the flexural strength and toughness of the beams under different temperatures? Is there any impact of different steel fiber dosage rate on the compressive strength?

3. How does the static elastic modulus of elasticity change with the steel fiber dosage rate? Is there any effect of temperature on dynamic elastic modulus?

1.3   Objective

The objective of this experimental work is to understand the effect of temperature and steel fiber dosage from subzero (in Celsius) to elevated temperature level. Therefore, this thesis aims to realize the effect of temperature on compressive strength, flexural strength, toughness, and modulus of elasticity. In conjunction, the relationship between modulus of elasticity, square root of compressive strength and theoretically obtained modulus of elasticity are developed.

1.4   Research Overview

The thesis is organized into five chapters. The first chapter describes the research background and motivation, research scope, problem statement, objectives, and research overview. The second chapter details a broad literature review that includes historical development of UHPC, impact of temperature on the mechanical properties of concrete and UHPC, effect of steel fiber on mechanical properties of concrete and fiber matrix interface. The third chapter includes the methodology of the experiments that involves outline of the experiment, material collection, mix design, mixing and specimen preparation, and test procedure. The fourth chapter includes all the obtained results. It also discusses the relationships among the test results along with the resulting tables and figures. Finally, chapter five draws the conclusion of the thesis and provides a future

direction. The material specifications, test results, mix proportions are shown in the appendices.

CHAPTER 2

LITERATURE REVIEW

This chapter represents a review of the existing literature about the effect of temperature and steel fiber on concrete mechanical properties. The review is divided into five sections. The first section outlines the background of ultra-high-performance concrete (UHPC). The second section reveals the effect of temperature on the mechanical properties of concrete. Consequently, the third section reveals the effect of fibers on concrete mechanical properties. The fourth section discusses the fiber-matrix interface. Finally, the fifth section summarizes the reviewed literature.

2.1   Development of UHPC

From the decades of evolution on concrete technology the term ultra high performance concrete (UHPC) has emerged. The definition of UHPC is still ambiguous. Yet, UHPC is typically comprised of Portland cement, silica fume, silica sand, steel fiber, superplasticizer, fine quartz powder and has a low water to binder ratio. The mixture does not contian coarse aggregate as is common with traditional Portland cement concrete mixes (Lee et al. 2007). The continual demand of this novel material has led to rigorous research. Until now many resaerchers have been trying to develop and optimize the design of UHPC from various perspectives.

A solid suspension model (SSM) to optimize high packing density of concrete has been presented by Larrard and Sedran in 1994 (F.de Larrard 1994). The authors established the model following Mooney's suspension viscosity model. Normal untreated

aggregates have been incorporated along with cement, silica fume and superplasticizer. In order to reduce the expense and to increase the feasibility, a simple thermal curing system has been employed. The study involved ordinary Portland cement that contains a little titanium oxide (C_3A) of 4.11%. The benefit of C_3A is to reduce the water requirement. Reduced carbon content improves the matrix fluidity. Such, a white silica fume has been employed. As a result, a cementitious matrix with 0.14 water binder ratio has been achieved. A meticulous selection of materials has been carried out to develop an optimal mix. Moderate viscosity and a low matrix final porosity has been observed to maximize the compressive strength. The authors reported a compressive strength of 34.2 ksi (263 MPa) with a simple thermal curing at 90^0C for 4 days (F.de Larrard 1994).

In 1995 Richard and Cheyrezy developed a ductile ultra high strength concrete based on granular components optimization, heat curing and pressure application (Richard 1995). The authors developed two types of reactive powder concrete (RPC) compositions: (1) RPC200 – comprised of steel fiber and without steel fiber similar to conventional concrete and (2) RPC800 – comprised of silica aggregates and steel agrregates along with compacting pressure. Upon the application of compressive load, the paste-aggregate interface tends to crack. Therefore, a homogeniety is paramount to develop RPC. In this study the homogeniety has been ctreated by replacing coarse aggregate with fine sand. Packing model has been incorporated to achieve the optimized granular mixtures. Thus, a densely packed cementitious mix has been developed. Confining pressure in the fresh concrete aided to develop even denser mix (e.g. RPC800) by removing entrapped air, extra water and shrinkage elimination. The heat treatment at

250^0C to 400^0C has led to form crystalline hydrates in RPC800 resulting in superb compressing strength. The authors envisioned RPC800 for hardening military structural use. Pozzolanic reaction seems to accelerate at 90^0C therefore, RPC200 has been heat treated under 20^0C-90^0C temperature. As a result, a ductile high strength concrete has been developed which generates three times lighter weight than conventional concrete structures (Richard 1995).

Vitek et al. (2013) developed steel fiber reinforced UHPC using locally available materials based on high density and low porosity of the constituent particles. The goal was to make a ready-mix concrete that would be delivered from mixing plant to construction site. Thirty concrete mixes have gone through the trial phases to determine an optimal mix. The packing has been optimized for each of the particles. The highest size of aggregate has eventually found to be 0.31 inch (8mm). The compressive strength test involved cylinders, cubes and fractions of beams after flexural strength test. Whereas, the flexural strength test has been incorporated with three different test methods. Although an anomaly has been noticed for different test methods, the authors reported an average compressive strength of 22.3 ksi (154 MPa) and 24.4 ksi (170 MPa) at 28 and 90 days respectively. The newly developed UHPC has been applied in a prestressed foot bridge. The authors also examined the anchorage zone test and pull out test. The examinations provided excellent results that made sure the safety and longevity (Vitek et al. 2013).

Soliman and Mamou (2017) developed an eco-friendy UHPC optimizing packing density of loaclly available granular materials, water/binder (w/b) ratio and water

reducing admixture (HRWRA) dosage incorporating statistical models. Four series of UHPC mix have been prepared based on different packing density (e.g. 0.75%, 0.77%, 0.79%, 0.81%) to investigate workability and compressive strength. Additionally, another ten series of UHPC mix have been made based on various w/b ratios (e.g. 0.15, 0.20, 0.25) and HRWRA. As the silica fume increased, the packing density also increased due to its small spherical glassy particles. Again, a linear decrease in viscosity has been observed with the higher packing density. This was due to the lubrication among the particles because of the addition of finer materials. Another reason was the increased yield stress due to the higher friction and compactness of the particles that resulted in decreased workability. Increasing of cement content seemed to have no significant effect on the compressive strength whereas the silica fume exhibited higher compressive strength and stiffness. To avoid the workability issue, the authors suggested an optimal packing density which is 0.79%. Higher water content showed a better flowability than higher water reducing agent because of improving HRWRA diffusion. Compressive strength at 28 days exhibited that the water content has seven times greater impact on strength than HRWRA. Finally, the authors proposed a design method to develop UHPC with locally available material by reducing the amount of cement and HRWRA that resulted 19 ksi and 26 ksi of compressive strengths. The proposed method also remarkably reduced the production cost and CO_2 emission (Soliman and Tagnit-Hamou 2017).

Wang et al. (2019) reported that the combination of D-optimal design and packing density methods are highly effective to develop UHPC. Given that both solid and liquid

phases could be modeled more accurately following this combined design approach. In this study, D-optimal design has been employed to establish a relationship between constituent particles and packing density. Based on the maximum packing density the packing particles have been evaluated. The authors noticed an optimized dosage of superplasticizer is the key to increase packing density. This is due to the decreased water film thickness and a better distribution of the solid particles. Theoretically, dense UHPC with low amount of cement and silica fume could be achieved by replacing them with lime powder. Thus, D-optimal design has been revealed to be an effective tool to develop eco-friendly and cost effective UHPC. The experimental validations have confirmed that at the optimized level the UHPC has the highest density, optimized pore structure, and superb compressive strength (Wang et al. 2019).

2.2   Effect of Temperature on Mechanical Properties

This section is divided into three parts. The first part depicts the effect of elevated temperature on the mechanical properties of concrete. The second part describes the effect of ambient temperature and the third part describes the effect of cryogenic temperature on the mechanical properties.

2.2.1   Effect of Elevated Temperature

In 2004, Poon at el. studied the mechanical properties of fiber reinforced high performance concrete (HPC) at elevated temperatures (Poon et al. 2004). The authors reported that at high temperature the compressive strength, toughness and stiffness reduced dramatically. They observed the mechanical properties of three mix series: plain

ordinary Portland cement concrete (PC), cement replaced by 20% metakaolin (MK) by weight and cement replaced by 10% silica fume (SF) by weight. Each of the series involved 0% fiber, 1% steel fiber, 0.22% polypropylene (PP) and 1% steel with 0.22% PP by volume. The compressive strength, toughness and stiffness were evaluated to three different temperatures: 20^0C, 600^0C and 800^0C. They reported that, in room temperature, due to the insufficient dispersion of PP fiber has a negative impact on the compressive strength while the steel fibers impact positively. While exposed to elevated temperature (e.g. 600^0C and 800^0C) the compressive strength reduced, on average, by 50% and 70% respectively. It is worth mentioning that steel fibers minimize the damage effects at high temperature. Another interesting observation has been made that although MK seemed to increase strength at room temperature it decreased the strength at elevated temperature. The reduction in toughness is comparatively less than compressive strength. Yet, steel fibers almost doubled the flexural toughness. On the other hand, the reduction in stiffness is quicker than reduction in compressive strength. Elevated temperature resulted only 18% stiffness retention at 600^0C with a further decrease of 11% at 800^0C (Poon et al. 2004).

Husem (2006) compared the behavior of ordinary (OMC) and high-performance concrete (HPMC) at elevated temperatures following unstressed residual strength test method. The unstressed residual strength test implies that specimens are heated without preloading at a prescribed rate until the thermal steady state is achieved. Then the specimens are allowed to cool at the room temperature at a prescribed rate prior to testing. The objective of the research program was to observe the compressive and

flexural strength of OMC and HPMC at elevated temperatures in different cooling environments (e.g. air and water). The authors investigated five different temperatures (e.g. 200^0C, 400^0C, 600^0C, 800^0C, 1000^0C). The OMC experienced higher loss in compressive and flexural test than HPMC, which showed higher resistance at high temperatures. Both concretes exhibited a common trend: a decrease in strength up to 200^0C then a slight increase from 200-400^0C and finally a gradual decrease after 600^0C. The study has stated that reduction in strength at elevated temperature is higher when the specimens are subjected to water cooling (e.g. 13% gain in air and 5% gain in water). During cooling in water, the specimens regained the evaporated moisture which has led toward the less removal of 'water of crystallization' (Husem 2006).

In 2019, Yang and Park realized the mechanical and thermal properties of UHPC exposed to high thermal cycles at 300, 400 and 500^0C (Yang and Park 2019). The research study was executed for three UHPC mixtures with the same volume fraction of polypropylene and three different (e.g. 1.0%, 1.5%, 2.0%) steel fiber percentages by volume. The study showed an overall decrease in compressive and tensile strength with the rising temperatures. The authors reported that the water in the matrix has been lost in between 300 and 400^0C and calcium hydroxide started to dehydrate at 500^0C. Therefore, the reported maximum decrease in strength is at 500^0C. Another observation has been made that the strength has increased with the higher steel fiber percentage. Similar decreasing trend has been observed in the case of unit weight and thermal conductivity with rising temperature. It has been observed that concrete behaves steadily after a sudden drop at 300^0C. Thus, inhibited a physical stability. It has been also noticed that

the steel fiber has no effect on the reduction of unit weight and thermal conductivity. A relationship has been established: at higher temperature compressive strength and thermal conductivity reduced due to the loss of unit weight. The scanning electron microscopy (SEM) and mercury intrusion porosimetry (MIP) analysis implied that the higher the temperature, the higher the porosity. Due to the different properties of steel fiber and cement paste the thermal expansion is incompatible which results in deterioration in the interfacial zone. Again, the polypropylene starts melting at 160^0C which leaves pores in the paste. Both of the scenarios are responsible for the reduction in mechanical and thermal properties of UHPC (Yang and Park 2019).

Ahmad et al. (2019) proposed emperical prediction models uisng analysis of variance method for compressive strength, flexural properties and modulus of elasticity in terms of exposure duration at the elevated temperature. The authors examined UHPC at elevated temperature in five different durations (e.g. 60, 120, 180, 240, 300 min) and with four steel fiber dosage by volume (2%, 4%, 6%, 8%) to understand the mechanical properties. The authors aimed to study the pre-spalling mechanical properties at 300^0C. The study reported an increase in compressive strength with a longer exposure duration. They have also observed a higher ductility along with the increment in steel fiber dosage. The scanning electron microscopy (SEM) image analysis exhibited progressive pozzolanic reaction that contributed to the increasing compressive strength at a diminishing rate. Moreover, the steel fibers prevented the progressive crack propagation in the matrix. However, flexural properties and modulus of elasticity have been observed to decrease with the duration of elevated temperature. The scenario has been explained as

the gradual deterioration of fiber matrix bond with the extended duration in temperature. The breakdown of the bond aided to the removal of moisture which eventually leads to the reduction in flexural performance (e.g. toughness index, flexural strength). Overall, the UHPC with low fiber contents have been affected less than those with higher fiber content (Ahmad et al. 2019).

In 2020 Li et al. carried out an investigation to realize the hybrid effect of polyethylene and steel fiber on the flexural performance of UHPC. The study represents a broad range of investigation on fiber hybridization, water-binder ratio, and aggregate size at ambient and elevated temperature (e.g. 300^0C and 600^0C). According to the study, the polyethylene fiber seemed to have a negative effect on compressive strength at room temperature. Whereas the steel fiber sets back the crack propagation and amplify the compressive strength. The hybrid effect of steel and polyethylene fibers decrease with water binder ratio and inclusion of larger aggregates has reported to improve the overall flexural performance. Based on the Field Emission Scanning Electron Microscope (FESEM) images both fibers have strong abrasion and load transfer capacity in between concrete paste and fibers. The authors suggested that the higher interfacial stress led to a higher tolerance in crack opening, which eventually improved the strain capacity. The inclusion of polyethylene fibers did not seem to improve spalling prevention at the elevated temperatures. Due to the lower coefficient of thermal expansion, the polyethylene fiber generated less cracks that is not enough for releasing vapor pressure. The flexural properties also deteriorated significantly after the exposure at elevated

temperatures due to melting of polyethylene fiber, loss of steel fiber matrix bond, and

mismatch in thermal expansion (Li et al. 2020).

2.2.2   Effect of Ambient Temperature

Berry et al. (2017) studied the behavior of beams under subzero temperatures (e.g.

20^0C, 0^0C, -20^0C, -40^0C) following four-point bending test. A total of four identical

beams were prepared with glass fiber reinforced polymers (GFRP). The report has shown

a linear elastic behavior until the first crack and the post cracking responses varied with

temperature. An improvement in both compressive and tensile strength has been noticed

with decreasing temperature. The authors reported a 40% increase in compressive

strength at -40^0C compared to 0^0C. Whereas, the tensile strength has experienced a sharp

increase from 20^0C to 0^0C. This phenomenon attributes to the formation of ice at cold

temperature. Ice creates bond with concrete matrix that leads to sustain higher imposed

load. Although, the ice tensile strength is barely sensitive to freezing temperature it

exhibits an increased compressive strength at decreasing temperature. All the beams

seemed to fail under glass fiber rupture; therefore, the ultimate capacity has not been

observed to vary remarkably (Berry et al. 2017).

2.2.3   Effect of Cryogenic Temperature

In 2018 Kim at el. investigated the mechaniacl and cracking behavior of fiber

reinforced UHPC before and after cryogenic attack (e.g. below -165^0C) applying energy

dispersive X-ray spectroscopy analysis. Four series of concrete specimens including

cylinders and edge-type slab specimens have been prepared to measure compressive

strength, cooling behavior, cracking behavior, and four-point bending test. The study

showed a higher crack resisting feature of UHPC compared to the normal concrete due to

its high strength matrix. Lower w/b ratio increases the tensile strength of UHPC and thus

the concrete's ability to withstand freeze thaw cycles. Addidtionally, the steel fiber in the

matrix prevents the crack formation and propagation. The authors noted that the

microcracks in the matrix exhibited a crack healing mannerism when subjected to

ambient temperature from cryogenic temperature. Results from scanning electron

microscopy and energy dispersive X-ray microscopy confirmed that the formation of

calcium carbonate ($CaCO_3$) crystal is responsible for filling the microcracks. Dissolved

carbon dioxide (CO_2) from air, carbonate (CO_3^{2-}) and bicarbonate (HCO_3^-) from carbonic

acid (H_2CO_3) dissipates with the free calcium ions (Ca^{2+}) and therfore the crystal of

calcium carbonate generates. This phenomenon also seemed to improve the flexural

performance of UHPC under cryogenic and ambient conditions. After exposure to

cryogenic cooling the flexural strength tend to increase by 16% over the general

specimens (Kim et al. 2018).

He et al. (2020) observed the flexural and compressive strength of UHPC under

cryogenic temperature based on different fiber types (e.g. steel fiber with three aspect

ratios, polyvinyl alcohol fiber, and polypropylene fiber). Four specimen groups with

different fibers has been involved in the research program with a temperature cycle from

20^0C to -170^0C. The authors noted that the specimens with steel fibers exhibited an

increasing flexural strength under cryogenic temperature due to the bonding effect of

concrete and steel fiber. The micro-morphological characteristic revealed that under the

cryogenic environment the smooth surface of steel fibers created a stronger bond with hardened cement matrix. While in the case of polyvinyl and polypropylene fiber, the flexural strength reduced by approximately 33% after cryogenic attack. This reduction attributes to the lower tensile strength and modulus of elasticity. The specimens experienced almost no variation in the compressive strength test before and after cryogenic attack. In the case of polyvinyl and polypropylene fiber, the results were worse. The authors suggested that, while recovering from cryogenic to room temperature the ice melts leaving a porous internal structure. Hence, the compressive strength deteriorates in the UHPC. To fully understand the microstructural characteristics an active acoustic emission test has been conducted. The result showed a lower damage variable in steel fiber filled specimens. The reason behind this phenomenon depicted that polyvinyl and polypropylene fiber absorbs water from cement hydration reaction, agglomerate together, which results in internal pores. This eventually leads to a higher damage variable (He et al. 2020).

2.3   Effect of Fiber on Mechanical Properties

2.3.1   Effect of Fiber Volume

In 2004, Song and Hwang proposed a model to predict compressive strength, tensile strength and modulus of rupture based on fiber volume fraction. The experiment was designed to observe the the mechanical properties of high strength steel fiber reinforced concrete at various fiber volume fraction level (e.g. 0.5%. 1% 1.5%, 2%) utilizing hooked-end steel fiber. For both of the tests (e.g. compressive and split tensile

strength) a gradual increment in strength was seen with the increasing steel fiber volume.

The maximum improvement of 15.3%, 98.3% and 126.6% was reported for compressive

strength, split tensile strength and modulus of rupture respectively. It is worth to noting

that the maximum compressive strength was found at 1.5% steel volume. The same

pattern of improvement has also been observed in toughness indices. The predicted

models for compressive, tensile strength and modulus of rupture are as followed (Song

and Hwang 2004):

$$f'_{cf} \text{ (MPa)} = 85 + 15.12 \, V_f - 4.71 \, V_f^2 \tag{2.1}$$

$$f_{tf} \text{ (MPa)} = 5.8 + 3.01 \, V_f - 0.02 V_f^2 \tag{2.2}$$

$$f_{rf} \text{ (MPa)} = 6.4 + 3.43 \, V_f + 0.32 \, V_f^2 \tag{2.3}$$

Where,

V_f = Steel fiber volume fraction

f'_{cf} = Predicted compressive strength, MPa

f_{tf} = Predicted split tensile strength, MPa

f_{rf} = Predicted modulus of rupture, MPa

Yoo et al. (2013) studied fracture and mechanical properties of UHPC at four

different micro steel fiber volume fractions (e.g. 1%, 2%,3%, 4%). Four series of test

specimens were prepared with steel fibers of 0.5 inch (13 mm) length and 0.007 inch (0.2

mm) diameter. The authors reported the maximum compressive strength at 3% fiber

volume fraction, which is mainly due to the confinement of fibers that delayed the micro

crack formation. At 4%, a higher decrease in strength has been noticed. This phenomenon

reveals that at higher steel fiber volume the concrete mix struggles to allot a homogeneous distribution. The peak load of flexural test seemed be affected largely by the increase of steel fiber volume. Whereas, first crack strength at the early phase of loading has been barely affected. This has been because the early strength is mainly drawn from the matrix strength. The fiber bridging property contributes to gains in the peak load even after experiencing multiple micro cracks after the initiation of first crack. Therefore, the fiber's pull-out behavior controls the strength after crack. At 2% steel fiber, the pull-out energy was exhibited to be the highest. Although the pull-out energy is depended on matrix strength, the result seemed to differ from maximum compressive strength at 3% steel fiber. The is because of the lower shrinkage of mix at higher steel fiber that creates radial confinement pressure in the matrix. Due to the bridging mechanism, the load deflection curve tends to create a tensile softening behavior. The authors proposed a tension-softening model at different steel fiber content from inverse analysis results, which aids to define failure mechanisms (Yoo et al. 2013).

Abbas at el. (2015) studied the mechanical properties and durability of UHPC with a varying steel fiber content (e.g. 1%, 3%, 6%) and length (0.31 in, 0.47 in, 0.62 in) with a micro-structural analysis. The steel fibers varied by volume adjusting quartz sand in the mix. In the study the compressive strength seemed to improve together with the steel fiber dosage. The authors realized that the steel fibers restricted the lateral expansion of the specimens which led to a higher load tolerance characteristic. The compressive strength and modulus of elasticity were also observed to improve with age because of the hydration reaction of the cementitious mix. For instance, the properties at 56 days were

shown to be strengthened by 6% and 8% respectively. However, the compressive strength variation along with fiber length was shown to be insignificant. Split tensile strength, flexural strength and toughness has also been observed to rise with accompanying increase in steel fiber volume. The rise attributed to fiber bridging action and a strong fiber-matrix bond. The investigation reported that short fibers (e.g. 0.31 in) prevent the development of micro crack and thus yield higher peak load and strain hardening behavior. After the peak, a steady drop has been noticed for micro crack development. It is due to the easier debonding characteristic of the short fibers. On the other hand, the long fibers (e.g. 0.62 in) performed better under debonding action and therefore, they exhibited strain softening behavior after the peak. Besides, crack width and porosity both have also been seen to decrease with higher fiber volume. Even with the lower porosity the durability seemed to improve without an effect of the fiber length (Abbas et al. 2015).

Wang and Gao (2016) observed entrapped air content and mechanical properties of UHPC at four different fiber contents (e.g. 0%, 1%, 2%, 3%) following statistical analysis. The study additionally focused on superplasticizer dosage and water to binder ratio (e.g. 0.18, 0.20, 0.22, 0.24). The authors reported a 4% - 6% air content at different steel fiber content which was much higher than normal concrete. Again, a sharp decrease in air content with the increment of fiber volumes has been observed. At high superplasticizer dosages, the micro fibers tend to distribute homogeneously. Therefore, higher steel fiber along with high superplasticizer dosage seemed to be responsible for continual lowering of air content. Compressive strength appeared to increase with higher steel fiber volume. At 0.18 w/b ratio the compressive strength increased by 59.1% for

0%-3% fiber. Higher steel fiber reduces the gap between fibers, that aids to sustain higher loads. Additionally, steel fibers prevent the crack propagation and crack generation. The reduction in air content also cooperated to improve the strength. At 1% steel fiber volume flexural strength seldom increased. However, 2%-3% fiber volume have experienced a dramatical improvement in strength due to stronger fiber matrix interlock (Wang and Gao 2016).

2.3.2   Effect of Fiber Shape and Type

Wu et al. (2016) focused to better understand the compressive and flexural behavior of UHPC with varying steel fiber shapes (e.g. straight, corrugated, and hooked-end) and volumes (e.g. 0, 1%, 2%, 3%). The fibers have the length of 0.51 inch (13 mm) and diameter of 0.0078 inch (0.2 mm) with a tensile strength of 406 ksi (2800 MPa). The random distribution of the steel fibers and the friction generated by the deformed fibers reduced the flowability of the mix remarkably. With the increment of fiber volume, the compressive and flexural strength increased gradually. It has been stated that the increased fiber content delayed the formation and propagation of cracks, and consequently improved the strength. Among the three fiber shapes, the hooked-end fiber demonstrated the maximum compressive and flexural strength. As such, for the 3% hooked-end steel fiber the compressive strength increased by 59%. The authors emphasized that the hooked-end fibers provide better mechanical joint compared to others. The study stated the first crack at three different fiber content are similar because at the initial phase the load-deflection is mainly controlled by the concrete matrix. After the peak, the load is sustained by the fiber friction and bond. At 3% fiber content, the

peak strength was essentially the highest (e.g. 101.6%). Like strength, the hooked-end fiber showed the maximum peak at load-deflection curve compared to others. The maximum peak for hooked-end fibers at 3% content was reported to increase by 123.3% (Wu et al. 2016).

Raza at el. (2021) focused on fiber hybridization in reactive powder concrete (RPC). Three types of fibers were involved in the study (e.g. steel fiber, glass fiber, carbon fiber) and amalgamations between two of them have also been investigated. The carbon fiber individually inhibited the maximum compressive strength because of its high tensile strength and modulus of elasticity. Whereas, steel fibers showed better deflection for its characteristic to prevent brittle failure. Addition of steel fiber with carbon fiber seemed to show the highest strength compared to other hybrids. Steel fibers reduced the lateral strain of the specimens by acting as stirrups in column. Smaller fibers (e.g. 0.59 in steel fiber, 0.78-1.1 in carbon fiber) slowed down the early micro cracking and crack propagation leading to an improved load carrying capacity. Longer fibers contribute to the strength on the later stages of testing when smaller fibers have already done its part. The authors reported an improved modulus of elasticity for the fibrous specimens. They believe, it was because of higher degree of mechanical compaction that reduced the porosity. Steel fiber reinforced-RPC and steel-carbon fiber hybrid mix showed the maximum total compressive toughness compared to other fibers. They showed a 140% and 190% increase individually than normal RPC. They also exhibited the highest gain in split tensile flexural strength test. This gain attributed to the rougher surface of steel fiber than glass and carbon fiber. The rough surface of steel fiber prevents the slippage of

fibers under loading condition. The gain is 26.6% and 32.1% respectively (e.g. steel fiber

reinforced-RPC and steel-carbon fiber reinforced-RPC) for split tensile test and, 35.8%

and 38.9% for flexural strength test (Raza et al. 2021).

2.3.3   Effect of Fiber Orientation

Huang at el. (2018) developed an L-shaped device with a narrow opening to

control the steel fiber orientation of UHPC and observed improved mechanical

properties. The speciality of the narrow opening was a 0.039 inch (10mm) width for a 0.5

inch (13 mm) steel fiber. Therefore, the fibers tended to turn around horizontally. Eleven

series of mixtures have been prepared changing streel fiber fraction by volume (e.g. 1%,

2%, 2.5%) and water to binder ratio (e.g. 0.2, 0.22, 0.24). For compressive strength test,

direction of load was perpendicular to the fiber orientation. With the increase in fiber

content (e.g. 3% steel fiber and 0.24 W/B ratio) the strength improvised by 29.6%. The

authors noticed a slight improvement in strength with the orientation of fiber and

therefore, they implied that the compressive strength is mainly dependent on fiber content

and water to binder ratio. The flexural strength and toughness have enhanced

dramatically. At 1% fiber content the flexural strength and toughness demonstrated the

maximum increased by 55% and 65.1% respectively. Before the peak load occurred at

load-deflection curve the strength directed due to matrix strength rather than fiber

orientation. After the peak, fiber bridging played a significant role to sustain more load

with an increase in fiber content. More the fiber larger the fiber bonding area between

fibers and concrete. Fiber orientation improved the strength provided that larger number

of fibers at the direction of tensile loading. (Huang et al. 2018)

Zhang at el. (2020) developed an imprvised device with vibration effect to align steel fiber in the UHPC mix. UHPC with high volume of steel fiber content is hard to flow due to the vicous force and yield stress, therefore, a vibration effect has been introduced to achieve additional workability. A channel (3.8 inch x 19.7 inch) made with stainless steel has been incorporated to cast UHPC by layers. Two mechanisms have been suggested regarding the fiber alignment: (1) the vibration table made sure the velocity gradient of the fluid which enables the fibers to flow parallel to the direction of flow and (2) the pull force of the channel ensured the parallel orientaition of fibers of fresh concrete. Two different steel fiber percentages by volume (e.g. 2%, 3%) and fiber shapes (e.g. straight 0.31inch steel fiber, hooked-end 0.51 inch steel fiber) have been included to study the mechanical properties of UHPC. The flexural test showed a slight rise (e.g. 18.5%) in the ultimate strength at 3% hooked-end steel fibers compared to 2% hooked-end fiber. Whereas, the specimens with hybrid fibers (e.g. hooked-end and straight fiber) demonstrated a relatively higher ultimate stregnth of 13.8% compared to 3% hooked-end steel fibers. The authors implied that the hybrid effect of steel fibers attributed to the micro and macro level crack formartion and propagation. They also have observed the load-deflection curve experienced a sudden drop compared to individual fiber specimens because of the pull-out manner of small fibers in the matrix. A dramatical improvement has been noticed in the fiber aligned hybrid specimens. The ultimate strength seemed to improve by 70.6% along with a 74.2% increase in deflection. The improvement ascribed the alignment of fibers along the direction of tensile stress. Direct tensile test has experienced 66% rise in ultimate strength similarly. Fiber aligning aided to develop

enough cracks and ductility until the ultimate strength has been reached. The fibers

continued to slip until they completely pulled out from the matrix before reaching the

main crack. Thus, a higher initial cracking strength has been observed. Fiber alignment

allowed an even distribution of fibers at the cross section that cooperated to achieve

better mechanical properties. However, the interlayer zones also created weak areas due

to fiber agglomeration. (Zhang et al. 2020b)

2.4   Fiber Matrix Interface

Tai and Tawil (2019) realized the twisted steel fiber pull out performance in

UHPC. The auhtors established finite element models for UHPC matrix, twisted steel and

interfacial bond to investigate the interfacial friction behavior. Both the aligned and

inclined fibers have been investigated to figure out the pull out characteristics of the

fiber. The study showed at higher pitch the steel fibers developed lower pull out force and

bond shear stress due to the twisted ribs per unit length of the fibers. This phenomenon

causes higher frictional resistance. Additionally, the twisted fibers exhibit slip-hardening

behavior which is responsible for the development of multiple cracks in UHPC. The

authors noticed, a great extent of pull out force has been maintained up to a large slip

distance, which has been almost 70%-90% of the embedded length. The "wedging effect"

of the twisted fibers and continual untwisting effect seemed to be liable for this greater

pull out force. Again, the rise in pull out force ascribe shorter pitch. The untwisting

mechanism of the shorter pitch might lead to fiber breakage and matrix spalling, which

caused significant energy dissipation (e.g. around 80%). Thus, the twisted fibers lose its

beneficial characteristics in improving mechanical properties. Higher embedment length

seemed to benefit this phenomenon. Compared to 0.23 inch, a 0.39 inch embedment length demonstrated to improve the pull out load by 42%. Additionally, inclined fibers demonstrated a high slip hardening behavior. However, with the increase in angle the slip hardening has been deteriorated (e.g. more than 45^0) (Tai and El-Tawil 2019).

In order to understand the fiber matrix bond, the study of interfacial transition zone (ITZ) is paramount. Weimer at el. (2020) studied the ITZ between fiber and the concrete matrix of UHPC with three different fibers (e.g. brass coated steel fiber, SF, stainless steel fiber, SSF, nitinolshape memory alloys, NiTi). The bond between fiber and cementicious matrix largly depends on the adhesive interaction, and shear and friction bond. During the pull out the adhesive bond, which originates from chemical interactions, controls the behavior. After the fibers experience debonding, the friction bond starts to control the overall fiber slippage. The entire event is influenced by the "micro-interlocking" of the fiber and matrix. Therefore, authors followed the tactic to rough up the surface of the fibers with laser treatment and incorporated scanning electron microscopy (SEM) to better understand the morphology. The study showed that the bond behavior largely depends on the alloy composition. For instance, brass coated steel fibers, without laser treatment, showed the maximum pullout stress over the others and a steady decrease of pullout stress around the "friction bond regime". Whereas, SF usually show a low slip dropping. The treated fibers showed the maximum bond stresses. Roughened surfaces tended to enlarge the bonding surface and thus improvised the interlocking. The electron microscopy images revealed that SSF-matrix experienced the maximum bond strength so that a failure cone has been formed. Also, SF showed a comparatively smooth

surface with a larger SF-matrix bond than NiTi (Wiemer et al. 2020).

2.5   Summary

1   For nearly two decades UHPC has been a material of high research interest.
Researchers have been working rigorously on optimized design, superior
mechanical, cracking and durability properties. Great attention has been payed to
reduce manufacturing cost in order to make UHPC readily available in the
market.

2   Variation in temperature has a clear influence on UHPC. Compressive and
flexural strength, and modulus of elasticity largely vary with temperature change,
pore structure of concrete, and hydration reaction of cementitious material. At
elevated or below zero temperature (in Celsius) the fiber matrix bond is
noticeably affected, and due to the homogeneity in UHPC, the matrix bond
behaves in different manner compared to normal concrete.

3   Fiber's volume, shape, length and size affect the mechanical properties of UHPC
remarkably. The fiber matrix bond depends on the distribution of fibers,
embedment length, fiber alignment angle, and fiber matrix interfacial zone (ITZ)
characteristic. The peak strength and behavior of load deflation curve of UHPC
before and after the peak strength are noticeably controlled by the fiber
reinforcement.

4   Fiber matrix interlock depends on the friction and shear force between them. The
chemical and physical properties of fiber (e.g. steel and carbon fiber or twisted
and straight fiber) dominate the adhesive interaction and pull out behavior to a

great extent.

CHAPTER 3

METHOLODGY

3.1   Introduction

The objective of this experimental study is to investigate the mechanical behavior
of steel fiber reinforced Ultra-High-Performance Concrete (UHPC) under in service
operability, terrestrial, ambient temperatures. A non-proprietary mix is utilized to
specifically study the influence of the steel fibers on the mechanical behavior. Al-Sarfin
studied the mix component parametric behavior of non-fiber reinforced UHPC
successfully in 2019 (Sarfin 2019). This research program utilizes the baseline mix
utilized in that 2019 study. Five batches of specimens are prepared with different steel
fiber percentages. The materials also vary parametrically according to the variation in
steel fiber percentage. The compressive strength, static modulus of elasticity, and flexural
toughness of UHPC is evaluated at five temperatures reflective of the range of typical in-
service temperatures. Each specimen is conditioned at the specific temperature before
testing.

3.2   Outline of Experimental Program

The experimental program is designed to study the temperature effect on
compressive strength, flexural toughness and static modulus of elasticity of steel fiber
reinforced UHPC. Additionally, a variation in steel fiber dosage is also studied to observe
the corresponding effect on the mechanical behavior. Due to the heterogeneity in
concrete, fluctuation in temperature causes change in mechanical properties. Specifically,

Portland cement paste shows instability due to abrupt temperature change (Sadd at el.,

1996). Thus, it necessitates the research of the temperature effect on UHPC due to the

fact that UHPC relies on the strength of the cement paste matrix. Previously, a number of

researchers have shown interest in the temperature effect on concrete materials (Ma et al.

2015; Poon et al. 2004; Berry et al. 2017). Overall, it has been observed that the

mechanical properties improve at lower or below zero temperature in degree Celsius (He

et al. 2020). At elevated temperature the concrete experiences a significant decrease in

strength (Yermak at el., 2017). However, a slight increase has been observed from 100^0C

to 300^0C (Klamer, 2009). Steel fibers tend to prevent the propagation of cracks in the

concrete (Tai at el., 2011; Jin at el., 2020). Thus, steel fiber has been noticed to improve

the compressive strength (Yang and Park, 2019). In addition, an interesting observation

has been made that steel fibers almost double the flexural properties (Poon at el., 2004).

This thesis studies the ambient temperature ranging from -25^0C to 55^0C as shown in

Figure 3.1. This range of temperatures is typical of those experienced by in-service

structures. Differences in steel fiber dosage percentage is the secondary focus of this

experimental work. The fiber dosage amount is varied parametrically, and the remaining

mix component amounts are held constant. The mechanical properties considered in this

experiment are the compressive strength, flexural strength and toughness and modulus of

elasticity.
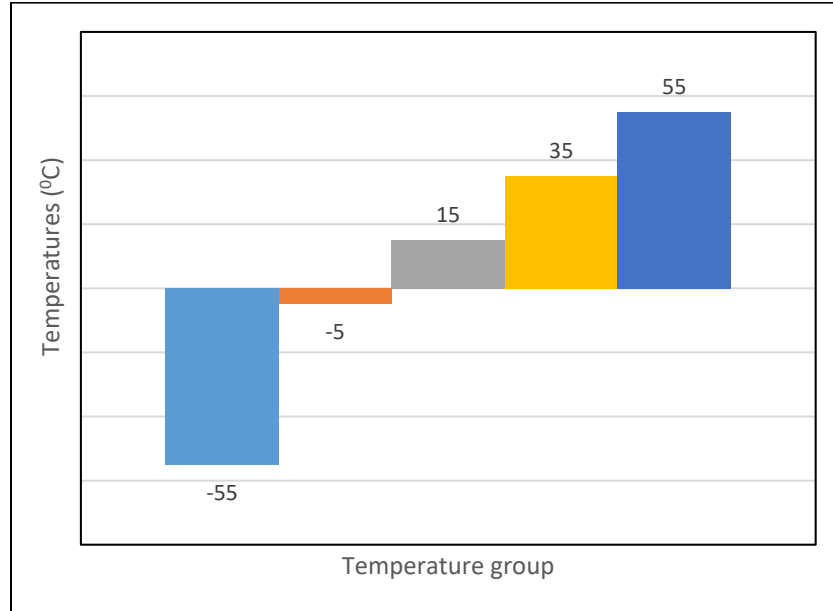
Figure 3.1: Graphical demonstration of five different temperatures

3.3   Material Collection

The concrete mix utilized in this research program is comprised of ordinary
Portland cement, silica fume, quartz sand, superplasticizer, and steel fiber. The ordinary
Portland cement is collected from Ash Grove Cement Company. The cement conforms to
the ASTM C150-16, Standard Specification for Portland Cement(ASTM 150, 2016) for
type II/III&V. Densified silica fume SF-100 is obtained from Master Builders Solutions.
The silica fume conforms to ASTM C 1240-15, Standard Specification for Silica Fume
Used in Cementitious Mixtures(ASTM 1240. 2015) Grade 4010 and 7030 quartz sand are
collected from Covia HLDGS Corp under the name of Granusil industrial quartz. In order
to achieve satisfactory workability, a full range water reducing admixture is employed,
specifically BASF Master Glenium 3030. The superplasticizer conforms to ASTM C494 /
C494M - 17, Standard Specification for Chemical Admixtures for Concrete (ASTM

C494, 2017). Steel fiber under the product name 5-13 is collected from Helix Micro-

Rebar. The steel fiber meets the specification ACI 318, Building Code Requirements for

Structural Concrete (ACI, 2005). The fiber used in this research are double helix micro

fibers (see Figure 3.2). The properties of the steel fibers are shown in Table 3.1.

Table 3.1: Properties of double helix steel fiber

Name of fiber	Length (inch)	Diameter (inch)	Coating	Tensile Strength (ksi)	Modulus of Elasticity (ksi)	Material
Helix 5-13	0.5	0.02	Electroplated Zinc	246.5	29000	High carbon steel

Figure 3.2: Double helix steel fiber (Helix Steel,2013)

3.4   Mix Design

The mix design is performed based on a previous parametric study of high

strength cementitious mixtures (Sarfin 2019). The research also followed the mix design

of a previous study of UHPC by Thomas and Sorensen (Thomas and Sorensen 2017).

Among the baseline mix, the steel fiber percentage is varied at an interval of 0.25%.

Based on the constant steel fiber percentage, proportion of silica fume, quartz sand,

cement, superplasticizer and water varied parametrically. Throughout the batches the

water to binder ratio is held constant at 0.2. Two types of quartz sand are incorporated:

Granusil 7030 and 4010. Both are sieved down to a No. 40 sieve. Therefore, the

maximum particle size is 0.0165 inches. Five groups of specimens are made

corresponding to five different testing temperature Each group contains five batches

based on steel fiber percentage. The temperatures at which the specimens are tested is

-25^0C, -5^0C, 15^0C, 30^0C, 55^0C. The five steel fiber percentages are 0.25%, 0.5%, 0.75%,

1% and 1.25%. The steel fiber percentages are calculated volumetrically. For the

compressive strength test, 3 inch diameter by 6 inch tall cylinders are prepared. However,

for modulus of elasticity 4 ich diameter by 8 inch tall cylinders are made. Additionally, 3

inch wide by 3 inch high by 12 inch long beam specimens are prepared for the flexural

strength test. The batch amount of the mix components is shown in Table 3.2.

Table 3.2:Mix Design Proportions of The UHPC Specimens

Steel Fiber (%)	Cement (lb/yd^3)	Silica Fume (lb/yd^3)	Water (lb/yd^3)	Sand[1] (lb/yd^3)	Superplasticizer (gal/yd^3)
0.25	2287.2	980.2	653.5	2061.6	9.75
0.5	2281.5	977.7	651.8	2056.4	9.73
0.75	2275.7	975.3	650.2	2051.2	9.70
1.00	2270	972.8	648.6	2046.13	9.68
1.25	2264.3	970.4	646.9	2040.96	9.65

*1:100% passing sieve size #40

The amount of dosage of each component varied parametrically keeping the

ration among them constant. The variation is shown in Table 3.3.

Table 3.3: Parametric variation of components based on the different in steel fiber volume

0.25% steel				
Materials (lb)	Sp.Gr.*	Quantity	Mix Ratio	Volume
Cement (C)	3.15	18.12	1.00	0.09
Silica Fume (SF)	2.20	7.77	0.30	0.06
Fine Sand (S)	2.65	16.34	0.63	0.10
Water (W)	1.00	5.18	0.20	0.08
HRWRA		0.65	0.02	
0.5% steel				
Materials (lb)	Sp Gr.	Quantity	Mix Ratio	Volume
Cement (C)	3.15	18.08	1.00	0.09
Silica Fume (SF)	2.20	7.75	0.30	0.06
Fine Sand (S)	2.65	16.30	0.63	0.10
Water (W)	1.00	5.17	0.20	0.08
HRWRA		0.64	0.02	
0.75% steel				
Materials (lb)	Sp Gr.	Quantity	Mix Ratio	Volume
Cement (C)	3.15	18.03	1.00	0.09
Silica Fume (SF)	2.20	7.73	0.30	0.06
Fine Sand (S)	2.65	16.25	0.63	0.10
Water (W)	1.00	5.15	0.20	0.08
HRWRA		0.64	0.02	
1% steel				
Materials (lb)	Sp Gr.	Quantity	Mix Ratio	Volume
Cement (C)	3.15	17.99	1.00	0.09
Silica Fume (SF)	2.20	7.71	0.30	0.06
Fine Sand (S)	2.65	16.21	0.63	0.10
Water (W)	1.00	5.14	0.20	0.08
HRWRA		0.64	0.02	
1.25% steel				
Materials (lb)	Sp Gr.	Quantity	Mix Ratio	Volume
Cement (C)	3.15	17.94	1.00	0.09
Silica Fume (SF)	2.20	7.69	0.30	0.06
Fine Sand (S)	2.65	16.17	0.63	0.10
Water (W)	1.00	5.13	0.20	0.08
HRWRA		0.64	0.02	

*Sp.Gr: Specific Gravity

3.5   Mixing and Specimen Preparation

The mixing procedure of UHPC differs from that of conventional concrete. Silica fume, quartz sand and cement are mixed in a mixing bowl thoroughly in the beginning. The mix is blended again to achieve a uniform mix in a rational cement mix machine sourced from Husky Tools. The model number used is GHM 105890 which operates at a speed of 25-27 rpm. The superplasticizer is mixed with water in advance. After a uniform mix has been achieved the mixture of water and superplasticizer is added to the concrete mix. The mixer machine is run continually until the desired consistency is achieved.

The specimens are prepared according to ASTM C192-19, Standard Practice for Making and Curing Concrete Test Specimens (ASTM, C192) following the exceptions in ASTM 1856-17, Fabricating and Testing Specimens of Ultra-High-Performance Concrete (ASTM, 2017). The cylindrical specimens are 3x6 inch for compression and 4x8 for modulus of elasticity. The beam specimens are 3x3x12 inches. The molds are filled in one layer. Instead of temping with a rod, the molds are tapped with a mallet 30 times. The specimens are covered with a plastic sheet within 1 minute of final preparation. The water binder ratio in UHPC is low and as such ASTM 1856-17 recommends covering the specimens as soon as possible. ASTM 1856-17 forbids the use of capping compound and the use of neoprene pads during test. According to ASTM 617-15, Standard Practice for Capping Cylindrical Concrete Specimens (ASTM C617, 2015) the capping materials are based on gypsum or Sulphur which are not compatible with the strength of UHPC. Alternatively, it is suggested to grind the end surface perpendicular to the axis not

exceeding more than 0.5^0. Therefore, all the specimens are ground according to the standard. The steps of the preparation process are shown in Figure 3.3.

Figure 3.3: Preparation of specimens

3.5.1 Mixing and Curing of Specimens

In the mixing phase the amount of superplasticizer is determined using a trial and error process. After several trials the amount of superplasticizer is achieved, which is 3.5 times of the designed dosage. The mixing and curing procedure (see Figure 3.4) are as follows:

1. Weigh the cement, silica fume, and quartz sand.

2. Mix them together uniformly for 2-3 minutes in a bowl.

3. Weigh water and superplasticizer and mix them together in a jar.

4. Pour the dry mixture into the mixer machine and run the machine for 4-5 minutes until the mixture is mixed thoroughly.

5. Add the mixture of water and superplasticizer into the mixer machine.

6. Keep the machine running for 5 minutes.

7. Stop the mixer machine and check the consistency.

8. Run the machine again for 5 minutes.

9. Stop the machine and check the consistency.

10. Run the machine again. The total time in the mixer machine is 15 minutes before it is finally stopped.

11. Pour the concrete into the 3x6 inch and 4x8 inch cylindrical and 3x3x12 inch beam molds. Fill the molds in one layer and tap with a mallet for 30 times.

12. After finishing the top surface of the specimens cover them with a plastic sheet within 1 minute.

13. Leave the mold for 24 hours before demolding. After demolding submerge the specimens into the lime water bath at 50^0C (122 ^0F) for 25 days.

14. After 25 days remove the specimens from the water bath and place them in the oven at 250^0C (482 ^0F) for 72 hours.

15. Remove them from the oven and condition them in the freezer at -25^0C, -5^0C, 15^0C, 30^0C, 55^0C for 48 hours. After 48 hours cool them down in the room temperature for 24 hours.

16. Test compressive strength, flexural toughness and modulus of elasticity.

Figure 3.4: Curing in the lime water bath, curing in oven and conditioning in freeze thaw chamber

The mixing and curing process is also summarized in Figure 3.5.
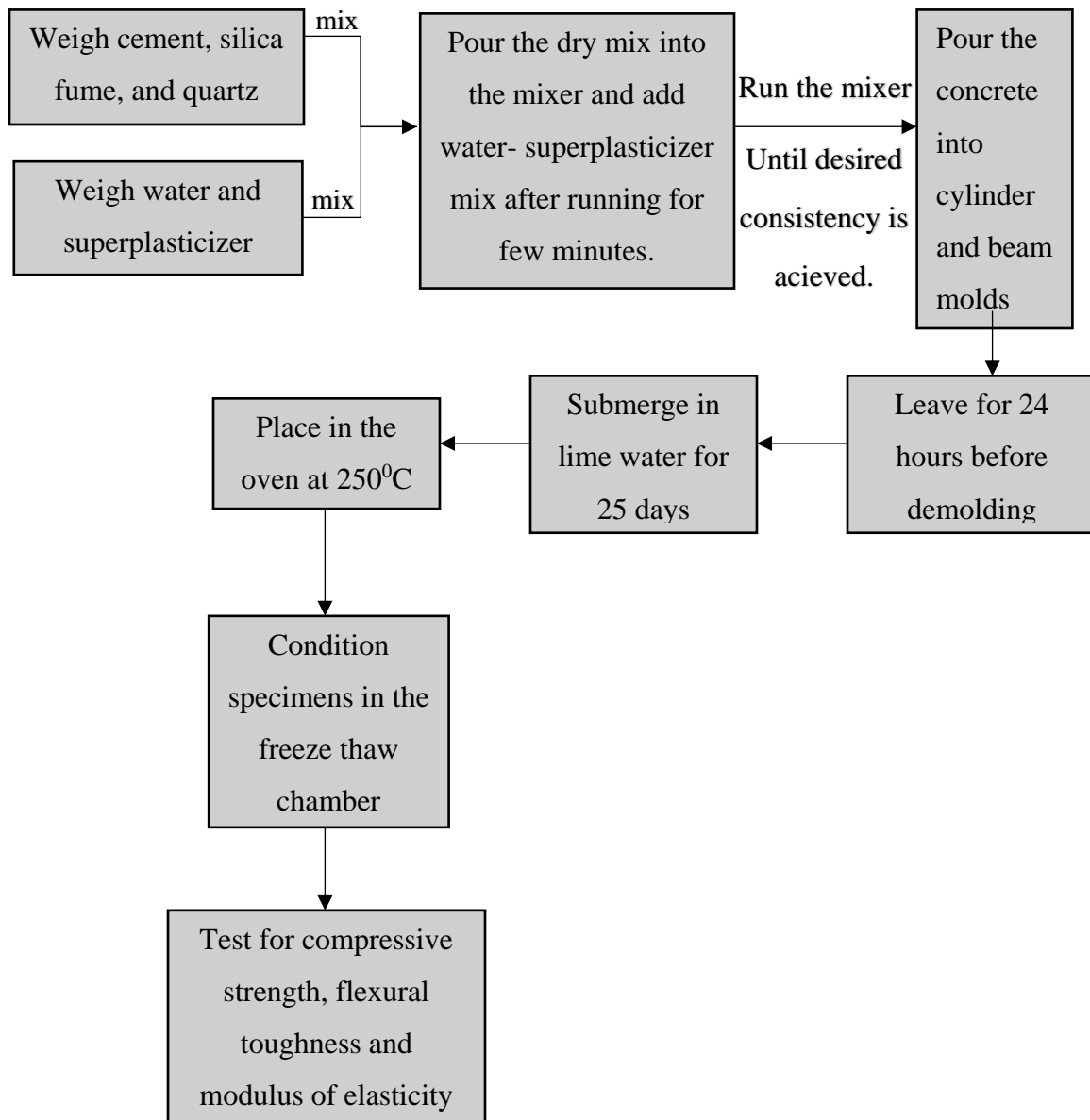
Figure 3.5 Mixing and curing of specimens

3.6   Test Procedure

The test procedures utilized in this study are described in the subsequent sections. The results of these tests are presented in later chapters.

3.6.1   Compressive strength Test

The compressive strength is calculated as the peak measured load divided by the average cross-sectional area. The specimens' length and dimeter are measured in order to calculate the average cross-sectional area. Prior to the measurement the end surfaces of the specimens are grinded precisely following ASTM 1856-17, Fabricating and Testing Specimens of Ultra-High-Performance Concrete (ASTM, 2017). The compressive strength test is employed following ASTM C39-15, Standard Test Method for Compressive Strength of Cylindrical Concrete Specimens (ASTM, 2015). The applied load rate for the UHPC specimens is set at145±7 psi/s. The strength of UHPC is significantly higher than conventional concrete. Therefore, the applied loading rate is faster than prescribed in C39-15.

For compressive testing, a Universal Testing Machine (UTM) is employed. The UTM is manufactured by Tinius Olsen has a capacity of 300 kips. The data collection software is from Instron under the name Partner. The software setup is prepared as a load-controlled setting. The load is applied up until the specimen can resist 80% of the applied load. After the software setup the specimens are placed on the loading platen for compression testing. The load is applied continuously, and without shock. The load is applied until the software records a decrease in loading and a clear fracture pattern. The

software shows the results as load at break and position. The peak load is utilized in the

compressive strength calculation. The compressive strength test setup color coded

specimens are shown in Figure 3.6.

Figure 3.6: Compressive strength test set up and cylinder specimens

From each of the batches, 5 cylinders are tested for the compressive strength.

Therefore, a total number of 25 cylinders have been investigated from each temperature

group. Thus, in the entire experimental program total 150 3x6 inch cylinders have been

examined along with the control batch. The temperatures are organized in ascending

order. The number of specimens is listed as shown in Table 3.4.

Table 3.4:Quantity of The Cylindrical Specimens for Compressive Strength Test.

Temperature group for cylinders	Steel fiber percentage (%)				
	0.25	0.5	0.75	1.00	1.25
C0	5	5	5	5	5
C1	5	5	5	5	5
C2	5	5	5	5	5
C3	5	5	5	5	5
C4	5	5	5	5	5
C5	5	5	5	5	5

*C0: Control Batch at 20^0C, C1: -25^0C, C2: -5^0C, C3: 15^0C, C4: 35^0C, C5: 55^0C

3.6.2   Flexural Toughness Test

The toughness is defined as the area under the load deflection curve. The area implies the energy absorption capacity of the specimens, which depends directly on the geometry of the specimens. The calculations to determine toughness are carried out according to ASTM C1018-97, Standard Test Method for Flexural Toughness and First-Crack Strength of Fiber-Reinforced Concrete (Using Three Point Bending) (ASTM, 1997). The ASTM C1018-97, in turn, refers to ASTM C78-15, Standard Test Method for Flexural Strength of Concrete (Using Simple Beam with Third-Point Loading) (ASTM, 2015). The ASTM C78-15 provides the loading rate of the three-point bending test based on the specimen size. Following ASTM C78-15, the range of loading rate is from 5.625 lb/sec to 7.875 lb/sec for this experiment. The loading rate utilized in this study is taken at 6.667 lb/sec.

The length, width and depth are measured for the necessary calculations and a. average of multiple measurements is used. All of the beams are marked precisely at two of the supports and in the middle for the accuracy of the three-point bending test. The test is performed with a UTM, sourced from Tinius Olsen. The software named Partner, sourced from Instron is also employed. The test is designed as load controlled. The specimens are loaded continuously, and without shock until the breaking point has been reached. A dial indicator used to measure the deflection during loading. The plunger of the dial indicator indicates the deflection at a thousandth of an inch. The dial has been placed at the middle of the beam specimen in a manner so that it ensures the accuracy of the reading. The test setup is shown in Figure 3.7.
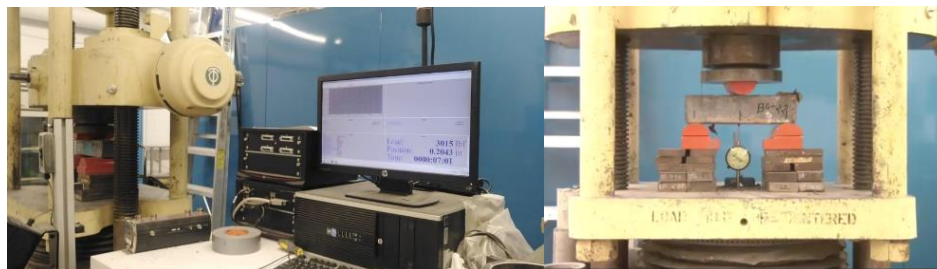
Figure 3.7: Three-point bending test set up

The deflection at the first crack point is identified which is used for the calculation of toughness indices. Toughness index represents the pattern of the material behavior. From each of the batches 3 beam specimens are tested. Hence the total number of 3x3x12 inch^3 specimens is 18 for each temperature group. In this work the total specimen count is 90 including all of the temperature group. The total number of specimens are broken down as shown in Table 3.5.

Table 3.5:Quantity of The Beam Specimens for Flexural Toughness Test.

Temperature group for beams	Steel fiber percentage (%)				
	0.25	0.5	0.75	1.00	1.25
B0	3	3	3	3	3
B1	3	3	3	3	3
B2	3	3	3	3	3
B3	3	3	3	3	3
B4	3	3	3	3	3
B5	3	3	3	3	3

*B0: Control batch at 20^{0}C, B1: -25^{0}C, B2: -5^{0}C, B3: 15^{0}C, B4: 35^{0}C, B5: 55^{0}C.

3.6.3   Static Modulus of Elasticity

Static modulus of elasticity is the slope of the stress strain plot measured during compression of concrete cylinders. The test is performed according to ASTM C469-14,

Standard Test Method for Static Modulus of Elasticity and Poisson's Ratio of Concrete in

Compression (ASTM, 2014). The loading rate is determined using ASTM 1856-17

(ASTM C1856 2017) and is considered at 145±7 psi/s. A compressometer is used to

measure to the nearest of 5 millionths of average deformation of two-gauge lines. The

effective gauge length is considered as one half of the specimen height. The

compressometer has two yokes: one is attached to the specimen and the other can rotate.

The length and diameter of the specimens are measured. The drill cores are made

following ASTM C42-20, Standard Test Method for Obtaining and Testing Drilling

Cores and Sawed Beams of Concrete (ASTM, 2020). The length of the drilled specimen

is measured according to ASTM C174-17, Standard Test Method for Measuring

Thickness of Concrete Elements Using Drilled Concrete Core (ASTM, 2017). The

modulus of elasticity test setup is shown in Figure 3.8.

Figure 3.8: Modulus of elasticity test set up

The specimen is placed on the lower platen with strain detecting device attached.

The obtained data from the first loading phase is not considered according to ASTM

C469-14. The load is applied continually, and without shock. The applied load is maintained 40% of the companion cylindrical specimens average ultimate load. The modulus of elasticity is calculated as follows:

$$E = (S_2 - S_1)/ (\varepsilon_2 - 0.000050)$$

Where,

E = Chord modulus of elasticity, psi

S_2 = Stress corresponding to 40% of the ultimate load

S_1 = Stress corresponding to a longitudinal strain, ε_1, of 50 millionths, psi

ε_2 = Longitudinal strain produced by stress S_2

The test is employed with modulus of elasticity testing machine from Humboldt model number BG3500-0-16. From each batch 3 cylindrical specimens are tested. Therefore, from each of the temperature group the number of 4x8 inch specimens is 18. A total of 90 cylinders are investigated for elastic modulus test including the control batch. The quantity of the specimens is as shown in Table 3.6.

Table 3.6:Quantity of The Cylindrical Specimens for Modulus of Elasticity Test.

Temperature group for cylinders	Steel fiber percentage (%)				
	0.25	0.5	0.75	1.00	1.25
M0	3	3	3	3	3
M1	3	3	3	3	3
M2	3	3	3	3	3
M3	3	3	3	3	3
M4	3	3	3	3	3
M5	3	3	3	3	3

*M0: Control batch at 20^0C, M1: -25^0C, M2: -5^0C, M3: 15^0C, M4: 35^0C, M5: 55^0C.

CHAPTER 4

EXPERIMENTAL TEST RESULTS

4.1   Introduction

This section presents the results of the experiments that are obtained following the

methodology described in Chapter 3. Compressive strength, flexural strength and

toughness, and static modulus of elasticity are measured at five different steel fiber

volumes, those are in turn categorized into five different temperature groups.

This chapter is divided into three major sections. The first section illustrates the

mechanical properties of UHPC. Which is also divided into three sub sections:

compressive strength, flexural strength and toughness, and static modulus of elasticity.

The next section presents the load deflection curves obtained during testing. A sub

section is included where, total energy absorption is calculated. The last section

established relationships between experimental and design values of modulus of

elasticity.

4.2   Mechanical Properties of UHPC

This experimental program is dedicated to realizing the compressive strength,

flexural strength and toughness and static modulus of elasticity of steel fiber reinforced

UHPC at subzero to elevated temperature (^{0}C). The steel fiber reinforcement dosage

amounts also vary parametrically throughout the experiment. Comparative strength test

results are reported along with correlations among them.

4.2.1   Compressive Strength

Compressive strength is investigated isolating both temperatures and steel fiber volumes. The temperatures range from -25^0C to 55^0C at a constant interval of 20^0C. Figure 4.1 shows compressive strength of UHPC along with standard deviations at five conditioned temperatures isolating five fiber percentages by volume. The trends of the plot show an overall decrease as the temperatures increase. The reduction in strength is somewhat lower at higher steel fiber percentage. For instance, at 1.25% and 1% steel fiber volume the slope of the tends are the lowest. From -25^0C to -5^0C, the compressive strength at 0.75%, 1% and 1.25% fiber content have experienced a slight increase. The increment in strengths are 1.23%, 13.91% and 6.4% respectively. After that, the compressive strength at each of the fiber volume have decreased until the subzero condition has ended. The maximum decrease has been recorded 31.5% at 1% steel fiber volume. The strength experienced a slight increase (e.g. maximum of 46% at 0.75% steel fiber) until 35^0C before decreasing again at 55^0C (e.g. maximum 33% at 1% steel fiber). The failure of the specimens was relatively ductile. An image of the typical failure is shown in Figure 4.2.

At subzero temperature the frozen water tends to create bond with the matrix interface therefore, the concrete is able to undergo higher sustaining load ((Berry et al. 2017). The microcracks in the concrete exhibit a crack repair behavior as the fiber matrix bond initiates. This could be the possible reason the for the higher strength trend at below zero temperature. The slight increase at -5^0C for the specimens with higher steel fiber probably because of higher fiber matrix bond. Because, as the fiber increases the bond

surface increases. Around 20^0C is known as a favorable temperature to accelerate cement hydrations process. Hence, the concrete gains strength in quicker manner (Kaleta-Jurowska and Jurowski 2020). This observation could be related with the overall increment in strength from 15^0C to 35^0C. As the hydration continues the porosity continues to increase (Lothenbach et al. 2007). As a result, the strength starts to experience a reduction, which is quite conspicuous on the later part of the plot. Due to having steel fiber reinforcement the concrete experiences a confinement that aids to prevent brittle failure. Since, the axial deformation is lower due to the lower lateral expansion. This observation agrees with the previously stated literature (Abbas et al. 2015).
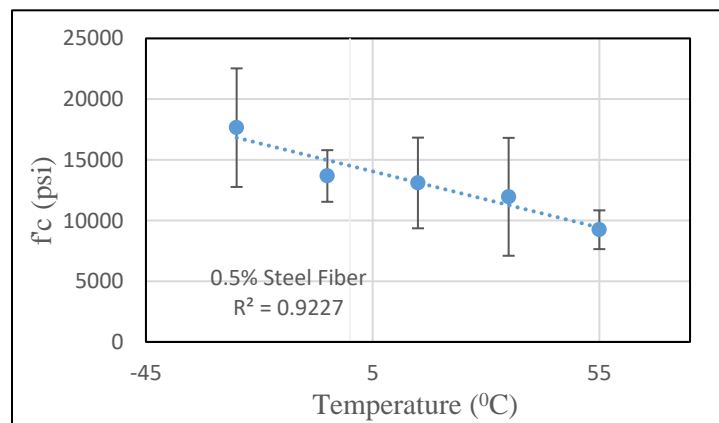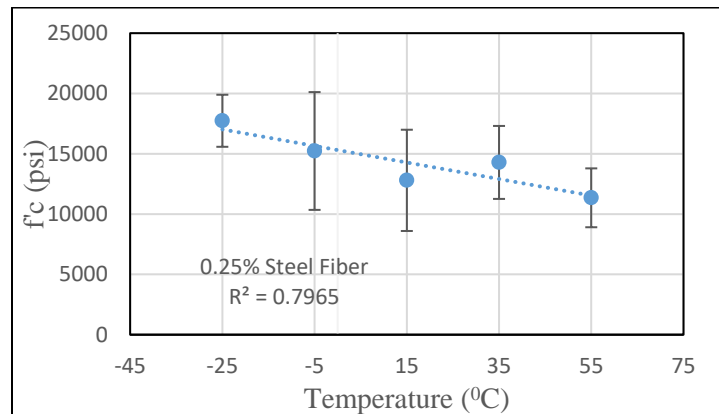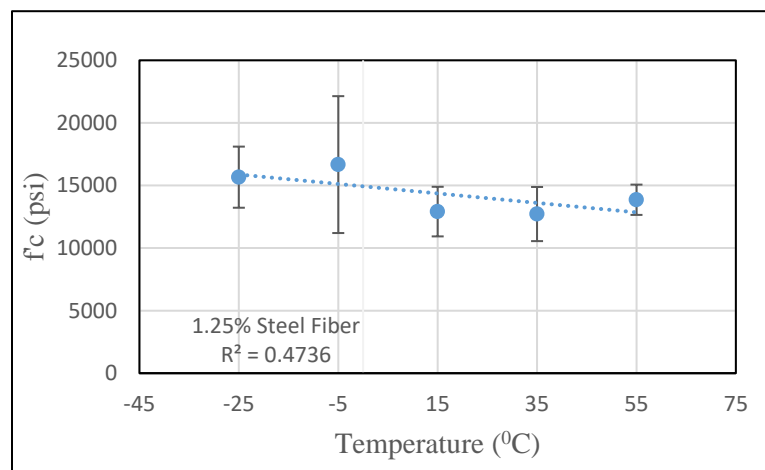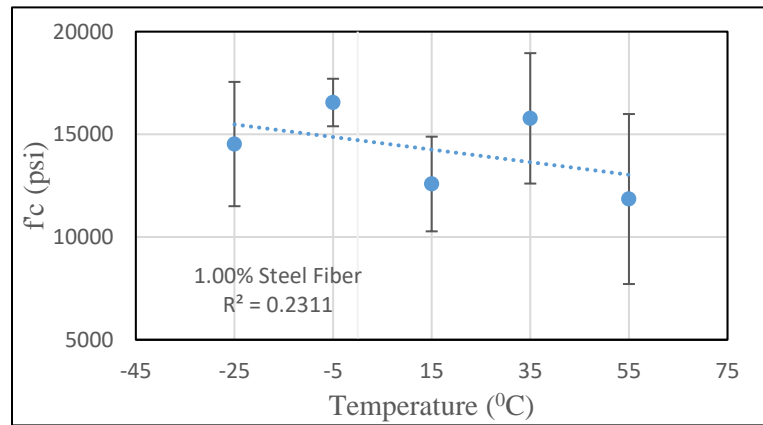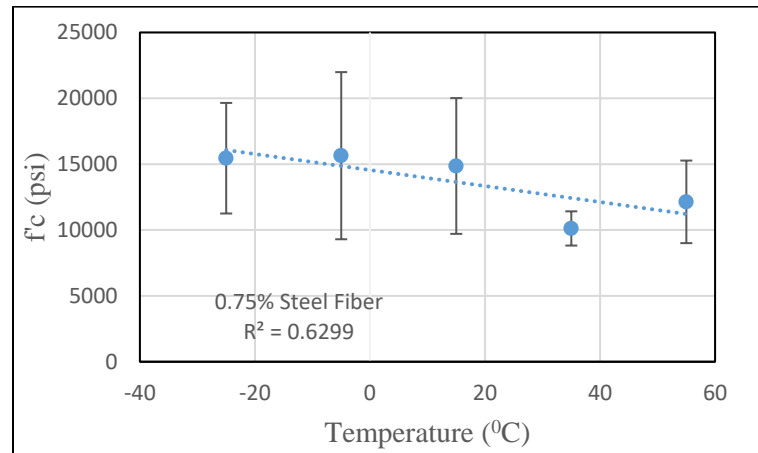
Figure 4.1:Variation of Compressive Strength with Temperature Isolating Steel Fiber Volume

Figure 4.2: Failure mode under compressive strength test

Figure 4.3 illustrates the variation of compressive strength at five different steel fiber volumes isolating temperatures. The plot depicts the compressive strength is somewhat insensitive with increase in steel fiber amounts. A slight improvement in strength is noticed from 0.5% to 1.25% steel fiber volume except at - 25^0C (e.g. a 13% decrease from 0.25% to 1.25%). The maximum increase is calculated to be 22% from 0.25% to 1.25% steel fiber at 55^0C. Alternatively, the strength has been observed to decrease slightly at 55^0C from 0.25% to 0.5%, where the maximum reduction has been noticed about 22%.

At the material level, steel fiber improves ductility and strength by developing friction bond between the fiber and concrete matrix (Wiemer et al. 2020). As the fibers are dispersed throughout the matrix they retard the crack propagation and the consenting path between fibers that consequently result in larger cracks. In higher steel fiber dosage the distance between fibers reduces, and thus they prevent more micro crack propagation and sustain higher load (Wu et al. 2017). The increasing trend in the compressive strength

with higher steel fiber aligns with this hypothesis. As mentioned earlier, at 55^0C the porosity of the concrete matrix is higher. Therefore, it is interesting to notice even at higher porosity, that the compressive strength experienced a rise with the increment in steel fiber. This phenomenon shows that steel fibers assist to reduce the influence of porosity in concrete. Only at -25^0C the strength seemed to reduce with the increment of steel fiber volume. This is probably due to the agglomeration in the steel fibers at higher dosage (Gao et al. 1997).
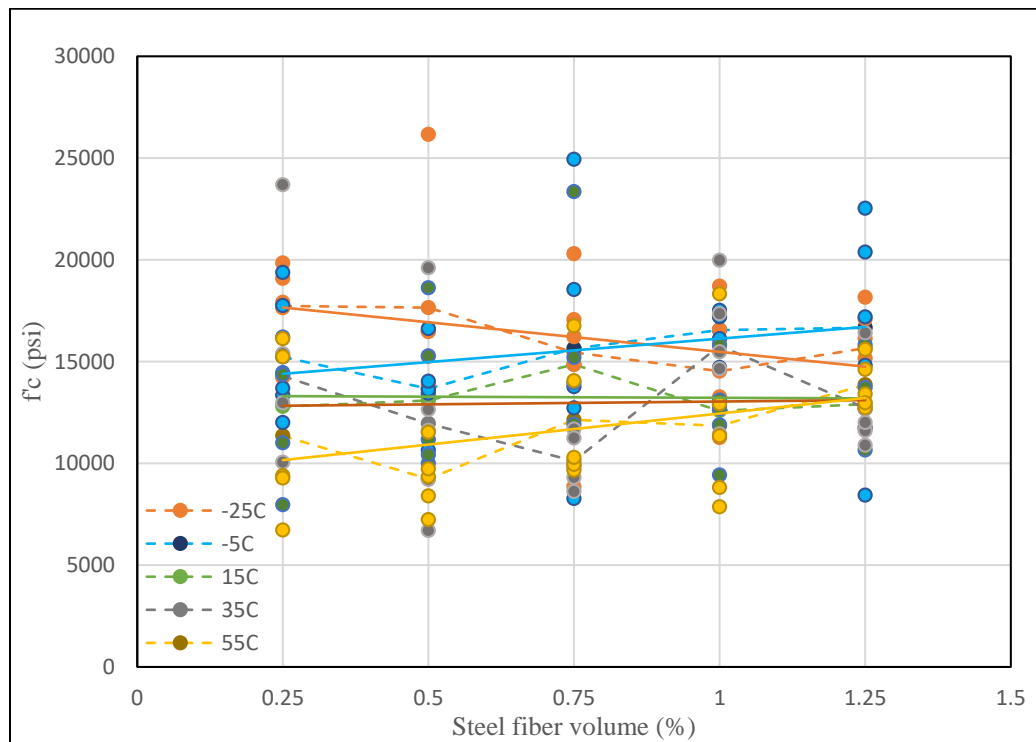
Figure 4.3: Variation of compressive strength with steel fiber volume isolating temperature.

A demonstration of compressive strength with and without steel fiber is presented in Figure 4.4. The test data are compared with the previous experimental work of Al-Sarfin, 2019 (Sarfin 2019). The scatter plot specifically shows the comparison of the

compressive strength with and without steel fiber. As plotted, the compressive strengths are dispersed around the 0% steel fiber line. The maximum strength is found at 0.75% steel, which is about 28.4% higher than 0% steel fiber specimen.
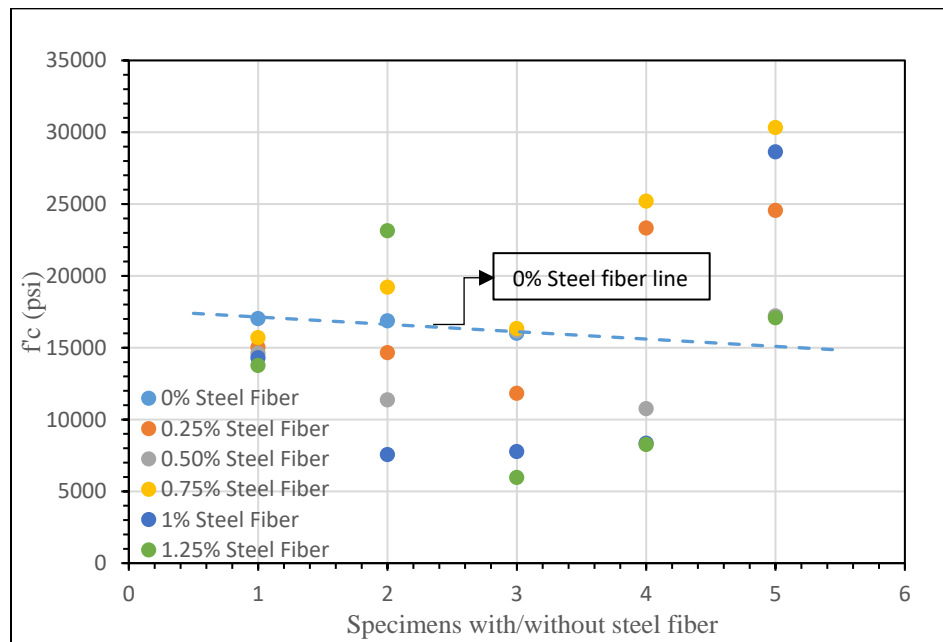
Figure 4.4: Comparison between compressive strengths with/without steel fiber

4.2.2 Flexural Strength and Toughness

Figure 4.5 shows the variation of flexural strength with temperature rise isolating steel fiber volume. Overall, a slight increase has been observed from -25^0C to 55^0C except for 0.25% steel volume. Maximum increment in strength has been exhibited at 0.5% steel fiber volume, which is a 35.5% increase (e.g. from 25^0C to 55^0C). In general, from 15^0C a slight improvement has been noticed up to -5^0C subzero temperature before decreasing at -25^0C (e.g. maximum of 35.5% decrease at 0.5% steel fiber volume). Again, at the elevated level, the strength has been increased overall up to 35^0C from 15^0C

(e.g. maximum 52.5% increase at 0.5% steel fiber volume). From 35^0C to 55^0C the strength is somewhat steady at each of the fiber volume content.

The free water in the concrete freezes at below zero temperature (e.g. freezing point of water is 0^0C). Therefore, the ice contributes to develop a sustainable matrix under load. As can be seen at -5^0C the strength has been experienced a slight increase from positive 15^0C. This event could probably be explained by the frozen water strength contribution. As the cement freezes the hydration reaction stops completely. The freezing point of Portland cement is around -4^0C depending on the ion concentration. Isolating the role of Portland cement at material level, the cementitious matrix experiences lack of hydration reaction and frost heaving (Zhang et al. 2020a). This could be a possible reason for the decreasing strength at -25^0C. From 15^0C to 35^0C temperature range, silica fume tends to form small amount of calcium hydroxide ($Ca(OH)_2$) than Portland cement. The small amount leads to lower formation of porosity and therefore, an improvement in strength could be observed (Cao and Detwilerl 1995). The rise in strength at 35^0C could be explained according to this mentioned hypothesis. UHPC contains very low water to cement ratio (e.g. 0.2 water to cement ratio in this experiment). With the acceleration in hydration reaction the free water in the cementitious matrix starts to disappear. At 55^0C the microstructure of concrete has almost lost its hydration product to accelerate hydration process. Therefore, from 35^0C to 55^0C a steady trend in strength has been observed without any noticeable fluctuation.
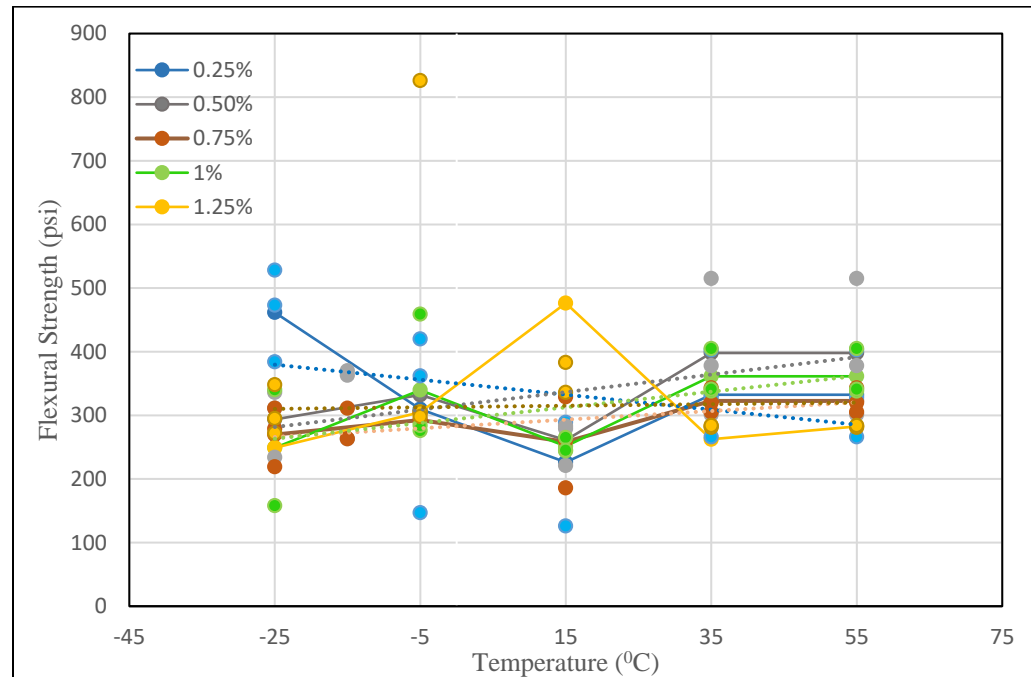
Figure 4.5: Variation of flexural strength with temperature isolating steel fiber volume

Figure 4.6 illustrates the variation of flexural strength with the steel fiber increment isolating temperatures. As the plot depicts, the differences in strength based on steel fiber content is subtle. From 0.25% to 0.5% a slight improvement in strength has been observed, where the maximum is 23.8% increase at 55^0C (NB. except for -25^0C). After that, a slight decline is conspicuous from 0.5% to 0.75% steel fiber volume at each of the temperatures (e.g. a maximum of 23.3% at 35^0C). An overall decline lasts up to 1% steel fiber volume before rising a little at 1.25% volume. At three temperatures (e.g. -5^0C, 15^0C, 55^0C) an overall increment has been noticed, where the maximum is 53.8% at -5^0C from 0.25% to 1.25% fiber volume. A ductile failure pattern is visible for all the specimens. Multiple micro cracks have been developed before they failed fully.

The steel fiber has been employed in this study is Helix 5-13 micro rebar. The constituent material of this fiber is high carbon steel wire electroplated with zinc. The

zinc coating provides a rough topography over the carbon steel surface. Therefore, it

enhances the strong interlocking between the fiber and concrete matrix. Thus, the fiber

bond should improve the mechanical property of the concrete (Sun at el. 2010). However,

the pullout of the micro fibers seemed to dominate the debonding from cementitious

matrix. One probable reason could be the fiber length (e.g. 0.5 inch) and alignment. With

smaller fiber length the embedment of the fibers is also smaller, which facilitate the

debonding (see Figure 4.7). Again, the higher alignment angle could cause slippage and

lower the load sustainability for not being able to resist the perpendicular load over the

specimen (Wiemer et al. 2020). Another reason could be the temperature effect. During

the variation in temperatures the concrete matrix undergoes several phases. Which leads

to different interfacial transition zones (ITZ). The way concrete matrix changes under the

variation of temperatures, the steel fibers do not exhibit that much variation at typical

service environment. Therefore, the interlock could be affected due to the changes in

matrix structure. For instance, the control specimen group (20^0C), which is not

conditioned, has exhibited a gradual rise in strength as the steel fiber volume increased.

The slope is about 175% higher than -5^0C slope, which is the maximum among all. In

general, the strength seemed not to be effected much by the steel fibers which is in

agreement with the literature that has said that, up to 1% steel fiber volume the change in

mechanical properties is subtle (Wang and Gao 2016).
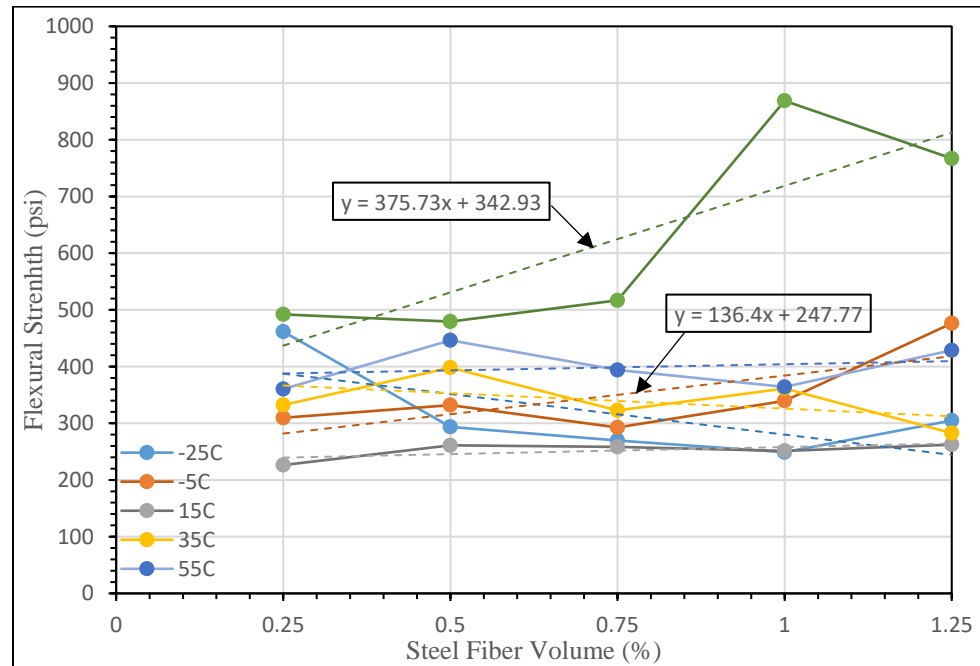
Figure 4.6: Variation of average flexural strength with steel fiber volume isolating temperature.

Figure 4.7: Failure pattern of beam specimen under three-point bending test

Figure 4.8 illustrates the variation of toughness with five different temperatures at different steel fiber volume. The toughness is calculated by integrating the area under load deflection curve, which is a measure of energy absorption capability of the beam specimens. The polynomial regression appeared to be the best fit for the data set

therefore, the plot depicts a nonlinear relationship between toughness and temperature. In this work, the toughness seems to improve at higher temperature level. Additionally, at steel fiber level, the maximum toughness has been attained at 0.75% steel fiber volume.

Toughness is essentially the area under first crack, which is mainly dependent on the fiber matrix bond. Comparatively higher toughness at 0.75% steel fiber volume implies a better anchoring between concrete matrix and fibers. The same upward trend has also been noticed at 0.5% and 1% volume level. Low steel fiber percentage such as 0.25% is most likely not enough to create necessary anchorage. Also, 1.25% fiber content probably creates congestion. The low amount of toughness indicates low first crack strength (e.g. at 15^0C). Mostly, the load deflection curves have started to generate micro cracks after the elastic zone. Although, the elastic behavior is not very remarkable in many of the specimens. Until the ultimate strength has been reached, the micro cracks kept propagating and a visible fiber bridging effect is noticed. Subsequently a sudden drop has been observed almost in every specimen after the ultimate crack. This phenomenon clearly depicts the benefaction of steel microfibers before the peak. The major benefit of the steel fibers is to help the specimens to sustain loading even after generation of multiple cracks. The steel fibers keep slipping before they are pulled out completely and thus aids to improve the ultimate strength as well as enlarged strain hardening zone. This event is easily discernable at the temperatures under 35^0C except some exceptions at -5^0C. At 35^0C and 55^0C the generation of microcracks declined dramatically and they are almost disappeared at 55^0C. The contribution of steel fibers has seemed not to be effective. Most of the specimens have shown the ultimate crack as the

first crack and a steady drop later on with a seldom softening zone. Which is the reason

of exhibiting higher toughness at elevated temperatures. This phenomenon also implies

that the toughness and strength correspond to the strength of cementitious matrix. The

reason of inadequate fiber matrix bond and especially the inefficient behavior of steel

fibers is not clearly understood. Therefore, this observation warrants further research.
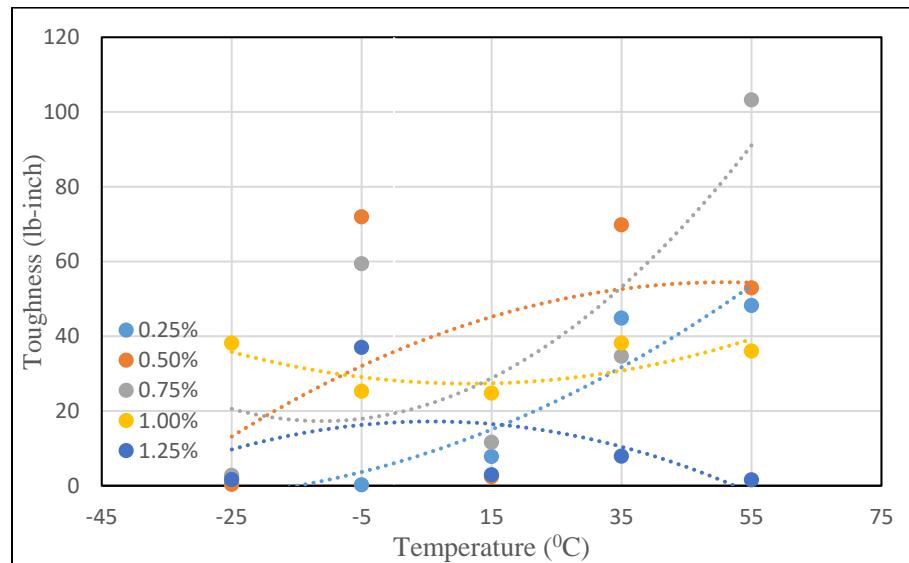
Figure 4.8: Variation of average toughness with temperature at different steel fiber
volume

4.2.3 Static Modulus of Elasticity

Figure 4.9 illustrates the variation of modulus of elasticity with temperatures

isolating steel fiber volume. An overall decline in modulus of elasticity has been

observed as the temperature increased. The slopes of the trends are somewhat similar.

The maximum slope at 0.5% steel fiber volume is only 9% higher than 0.25% volume. A

slight increase has been observed for 1% and 1.25% steel volume level at higher

temperature, which is only 3%. Previously, it was reported elsewhere that at lower

temperature (e.g. at -20^0C to 50^0C temperature range) modulus of elasticity increases

(Shoukry et al. 2011). Therefore, this experimental observation is in an agreement with the stated literature.
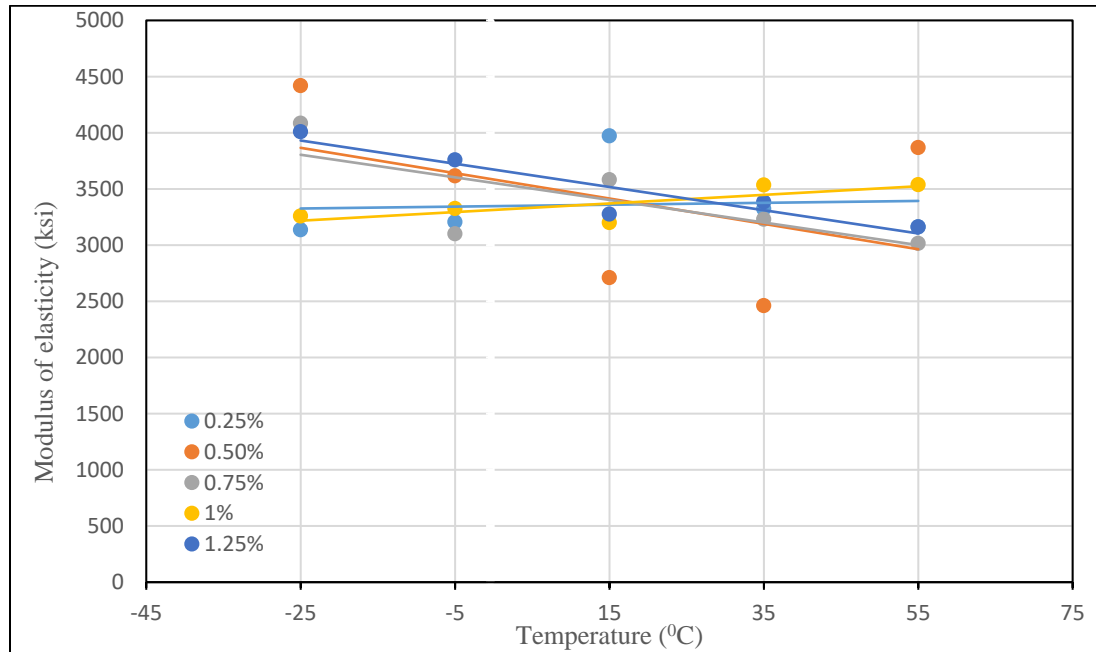
Figure 4.9:Variation of average modulus of elasticity with temperature

Figure 4.10 shows the variation in modulus of elasticity with steel fiber volume isolating temperature effect. A rise in modulus of elasticity has been noticed at -25^0C, -5^0C and 35^0C temperature level as the steel fiber volume increased. The maximum increase has been experienced at 35^0C, where the slope is 105% higher than -25^0C. Steel fibers aid to minimize the axial deformation of the specimens as the loading continues. The fiber matrix bond acts as a confinement under the compression load. Therefore, an improvement could be noticed in modulus of elasticity (Raza et al. 2021). This observation could be a probable reason for this rise. However, at 15^0C and 55^0C, the modulus of elasticity seemed to decrease with the increase in steel fiber content.
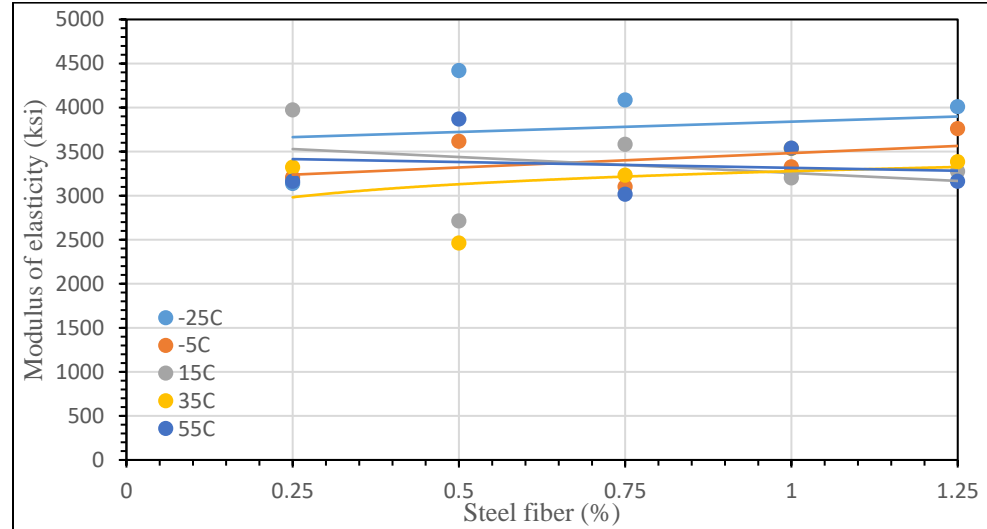
Figure 4.10: Variation of average modulus of elasticity with different steel fiber volume

4.3   Load Deflection Behavior

A typical load deflection curve is illustrated in Fugure 4.11. As can be seen, the initial phase of the curve developed a number of micro cracks that has led to the larger strain hardening zone. Small fibers tend to retard the micro crack development and the propagation in the matrix providing an effective crack generation. Therefore, they allow to sustain specimens longer before the macro cracks develop (Sheng, 1995). This hypothesis explains the portion of the curve before it reaches to its ultimate zone. From the initiation of hair line cracks, the more visible cracks contitued to grow as the loading increased. Throughout the loading phase, the specimens have continued to exhibit the fiber bridging property from little slippage of steel fibers to higher. Hence, fiber bridging seemed to contribute to a longer strain hardening zone. A steep drop after the peak has been noticed. This phenomenon indicates the pull out of the micro fibers. During the pull

out the smaller fibers started to debond probably for its lower embedment length.

Therefore, no improved softening zone has been noticed in general.
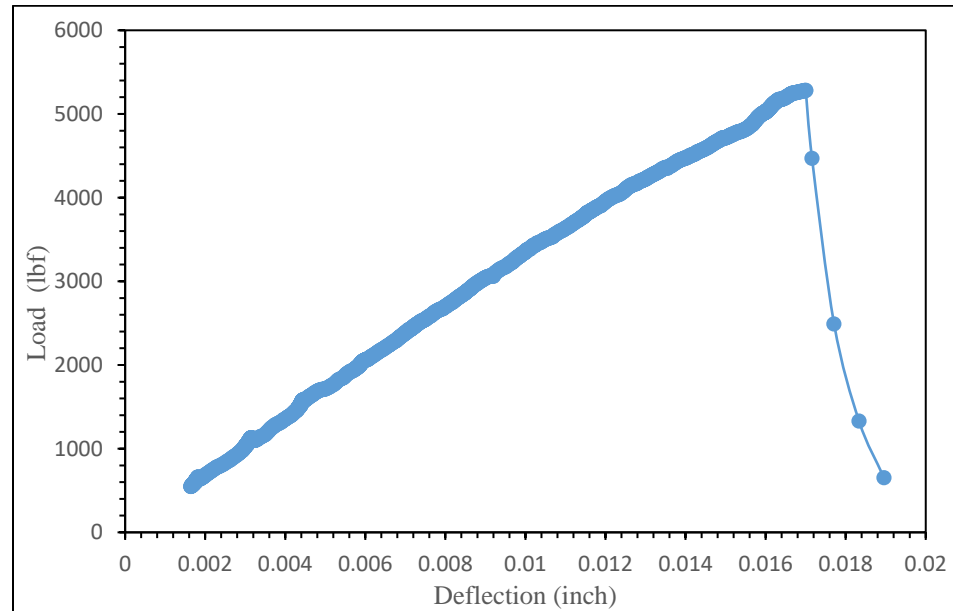
Figure 4.11: Typical load deflection curve

4.3.1 Total Energy Absorption

An approximation of ductility could be identified from the amount of total energy absorbed by the specimens. The total area under the load deflection curve until a complete failure indicates the total absorbed energy (Raza et al. 2021). Figure 4.12 shows the variation of total energy absorption with steel fiber volume content isolating temperature effect. The ductility of the specimens seemed to improve moderately with the rise in steel fiber volume. The maximum rise has been overserved at 55^0C, while the minimum is at -25^0C. At each of the temperature from -5^0C to 55^0C, the improvement is 67.57%, 78.79%, 23.41%, 52.57% respectively from 0.25% to 1.25% steel fiber volume. However, the maximum improvement has been observed at 1% fiber volume for -25^0C, which is 38.03% compared to 0.25% steel volume. At improved ductility stage the

amount of absorbed energy is higher, which indicates the larger area under the load deflection curve. This observation justifies that higher steel fiber volume improvises load sustainability (Wu et al. 2016).
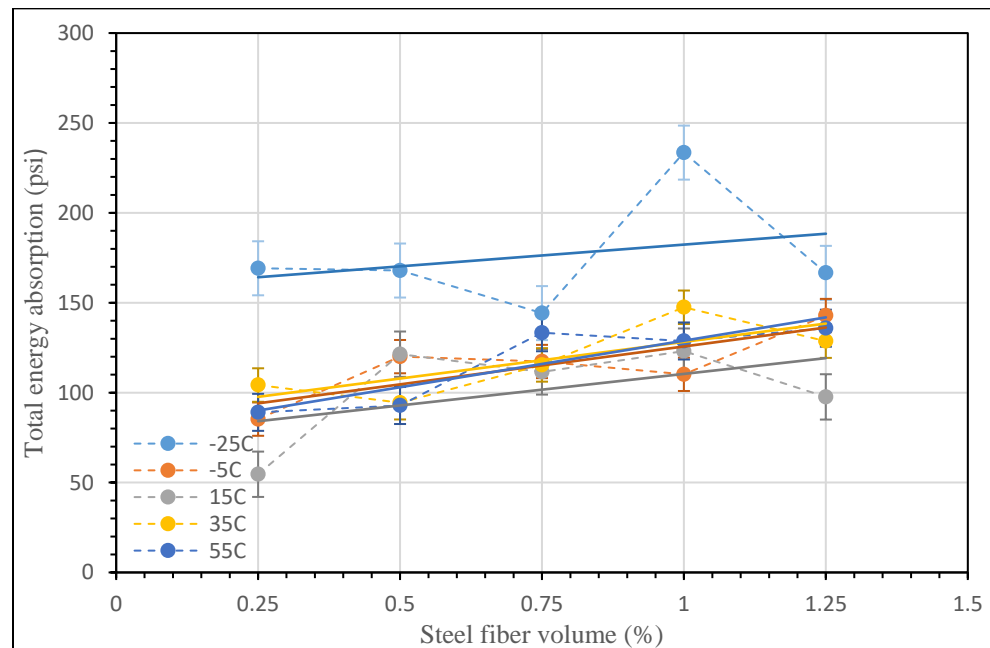
Figure 4.12:Variation of total energy absorption with steel fiber volume

4.4   Experimental and Design Value Relation of Modulus of Elasticity

This section provides two major relations: (1) relation between square root of compressive strength and elastic modulus of elasticity and (2) relation between experimental and design values of modulus of elasticity.

4.4.1   Relation Between Square Root of Compressive Strength and Modulus of Elasticity

The modulus of elasticity and square root of compressive strength are closely related to each other. The relation between modulus of elasticity and square root of

compressive strength is demonstrated in figure 4.13. At first relation has been established isolating effect of steel fiber. The relations are solved applying quadratic linear function.

$$P(x) = Ax + B \qquad (4.1)$$

The plot represents the square root of compressive strength test data and laboratory obtained modulus of elasticity at fiver steel fiber content. The linear relations are listed from 4.2 to 4.6.

$$MOE(ksi) = -12189\sqrt{f'_c} + 4812, \quad SF=0.25\% \qquad (4.2)$$

$$MOE(ksi) = 22080\sqrt{f'_c} + 898.26, \quad SF = 0.50\% \qquad (4.3)$$

$$MOE(ksi) = 19499\sqrt{f'_c} + 1132.4, \quad SF = 0.75\% \qquad (4.4)$$

$$MOE(ksi) = -166.8\sqrt{f'_c} + 3390.7, \quad SF = 1.00\% \qquad (4.5)$$

$$MOE(ksi) = 38900\sqrt{f'_c} - 1137.9, \quad SF = 1.25\% \qquad (4.6)$$
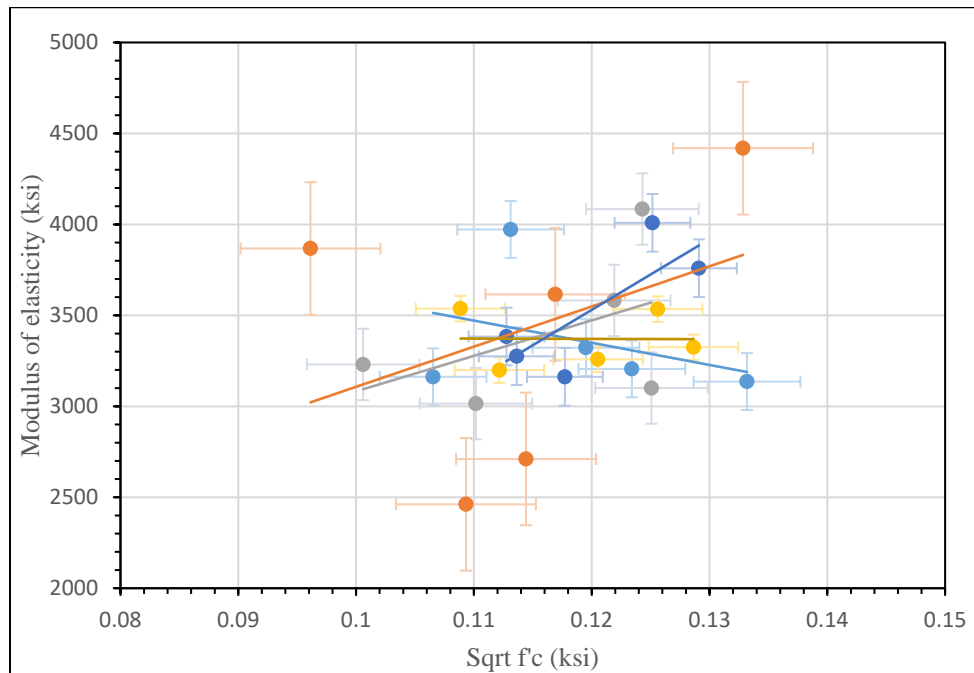
Figure 4.13: Relationship between modulus of elasticity and square root of compressive strength isolating steel fiber content effect

Figure 4.14 represents the square root of compressive strength test data and laboratory obtained modulus of elasticity at five different temperature conditions. The linear relations are listed from 4.7 to 4.11.

$$\text{MOE(ksi)} = 15125\sqrt{f_c'}1857.3, \text{T=-25}^0\text{C} \tag{4.7}$$

$$\text{MOE(ksi)} = -2625.8\sqrt{f_c'} + 3728.3, \text{T} = -5^0\text{C} \tag{4.8}$$

$$\text{MOE(ksi)} = 21681\sqrt{f_c'} + 853.39, \text{T} = 15^0\text{C} \tag{4.9}$$

$$\text{MOE(ksi)} = 20012\sqrt{f_c'} + 913.71, \text{T} = 35^0\text{C} \tag{4.10}$$

$$\text{MOE(ksi)} = -34016\sqrt{f_c'} + 7018.5, \ \text{T} = 55^0\text{C} \tag{4.11}$$
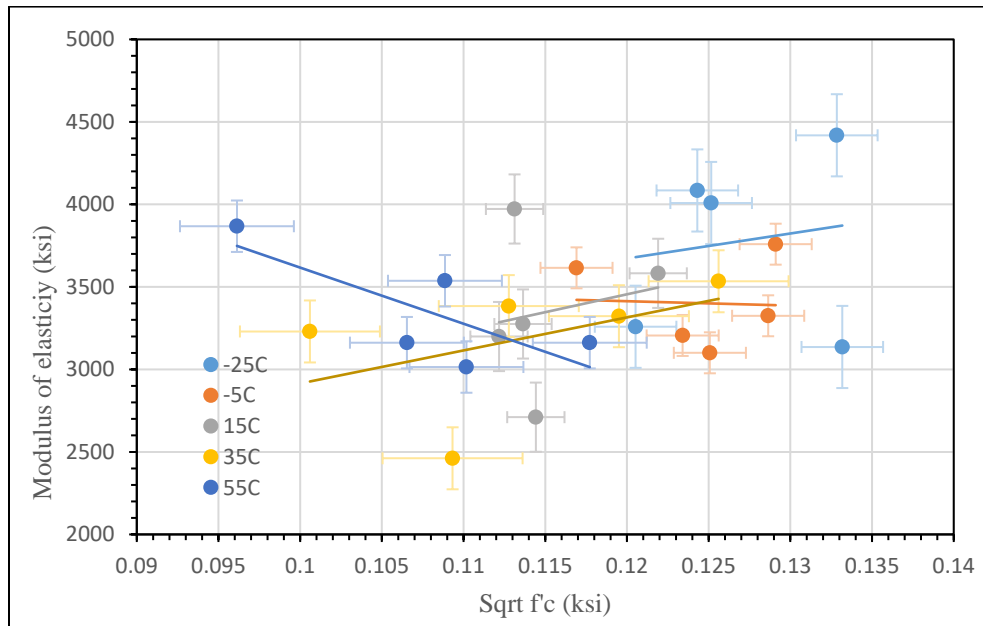
Figure 4.14: Relationship between modulus of elasticity and square root of compressive strength isolating temperature effect

As the plots depict, the data points are too scattered to predict an effective relationship. The trends are overlapping with each other, which has made the plots

ambiguous. However, in general, the relationships almost agree with the previous observation of modulus of elasticity with temperature and steel fibers effect. At lower temperature and higher steel fiber percentage the relationship between modulus of elasticity and square root of compressive strengths shows a higher trend. Additionally, modulus of elasticity has increased with the increase in compressive strength.

4.4.2 Relationship between Experimental and Design value Modulus of Elasticity

According to ACI 318-05 the modulus of elasticity (MOE) of normal concrete is given in 4.12.

$$E_c = 57000 \sqrt{f_c'} \text{ (in psi)} \tag{4.12}$$

ACI provides another relationship of MOE and compressive strength including unit weight of concrete that is given in 4.13.

$$E_c = 33 \, \rho^{1.5}\sqrt{f_c'} \text{ (in psi)} \tag{4.13}$$

The second relationship provides an estimation of MOE of concrete related to the unit weight ranging from 90 to 155lb/ft^3. Evidently, the unit weight of UHPC is different than normal weight concrete. Until now many researchers have been investigating to find a relationship of MOE (Graybeal 2007; Graybeal and Stone 2012; Ma et al. 2004). Federal Highway (FHWA) research program (Graybeal and Stone 2012) has proposed a relationship that estimates MOE of UHPC with a compressive strength ranging from 14 to 26 ksi given in 4.14.

$$E_c = 49000\sqrt{f_c'} \text{ (in psi)} \tag{4.14}$$

The research program was focused on different curing temperatures where they have found, the MOE mainly depends on compressive strength, not curing temperature.

Therefore, this portion of thesis represents relations between the modulus of elasticities obtained from laboratory experiment and the design value modulus of elasticity from Federal Highway (FHWA) research program (Graybeal and Stone 2012).

Based on temperature effect the equation stated in 4.14 varied in this work. A variation of the constant 49000 at different temperature along with different steel fiber level is shown in Table 4.1. The table clearly shows that all the constant values are well below the design constant. This is probably the influence of steel fiber's inefficiency and inadequate matrix strength.

Table 4.1:Variation in modulus of elasticity constant with temperature

Steel fiber (%)	Modulus of elasticity	Constant	Square root of Compressive Strength
$-25^{0}C$			
0.25	E=	23547.3436	$\sqrt{f_c'}$
0.5	E=	33262.0739	$\sqrt{f_c'}$
0.75	E=	32856.5886	$\sqrt{f_c'}$
1	E=	27034.5613	$\sqrt{f_c'}$
1.25	E=	32027.9586	$\sqrt{f_c'}$
$-5^{0}C$			
0.25	E=	25976.1074	$\sqrt{f_c'}$
0.5	E=	30924.5048	$\sqrt{f_c'}$
0.75	E=	24789.5667	$\sqrt{f_c'}$
1	E=	25846.1287	$\sqrt{f_c'}$
1.25	E=	29114.9767	$\sqrt{f_c'}$
$15^{0}C$			
0.25	E=	35114.346	$\sqrt{f_c'}$
0.5	E=	23688.8779	$\sqrt{f_c'}$
0.75	E=	29383.4265	$\sqrt{f_c'}$
1	E=	28520.6487	$\sqrt{f_c'}$
1.25	E=	28821.3823	$\sqrt{f_c'}$

35⁰C			
0.25	E=	27800.1443	$\sqrt{f_c'}$
0.5	E=	22513.3983	$\sqrt{f_c'}$
0.75	E=	32107.7906	$\sqrt{f_c'}$
1	E=	28136.6819	$\sqrt{f_c'}$
1.25	E=	30003.8977	$\sqrt{f_c'}$
55⁰C			
0.25	E=	29680.7544	$\sqrt{f_c'}$
0.5	E=	40233.8786	$\sqrt{f_c'}$
0.75	E=	27361.2808	$\sqrt{f_c'}$
1	E=	32492.0456	$\sqrt{f_c'}$
1.25	E=	26860.0564	$\sqrt{f_c'}$

The relations between experimental and design value modulus of elasticity are shown in Figure 4.15 and 4.16. The linear regressions are found as the best fit for the data set.

Figure 4:15 represents the relation between experimental and design value modulus of elasticity isolating steel fiber volume effect. The linear relations are listed from 4.15 to 4.19.

$$\text{MOE(ksi)} = -0.2488\text{MOE}' + 4812, \text{SF=0.25\%} \tag{4.15}$$

$$\text{MOE(ksi)} = 1.6764\text{MOE}' - 5668.2, \text{SF} = 0.50\% \tag{4.16}$$

$$\text{MOE(ksi)} = -0.0034\text{MOE}' + 3390.7, \text{SF} = 0.75\% \tag{4.17}$$

$$\text{MOE(ksi)} = 0.3979\text{MOE}' + 1132.4, \text{SF} = 1.00\% \tag{4.18}$$

$$\text{MOE(ksi)} = 0.7939\text{MOE}' - 1137.9, \text{SF} = 1.25\% \tag{4.19}$$
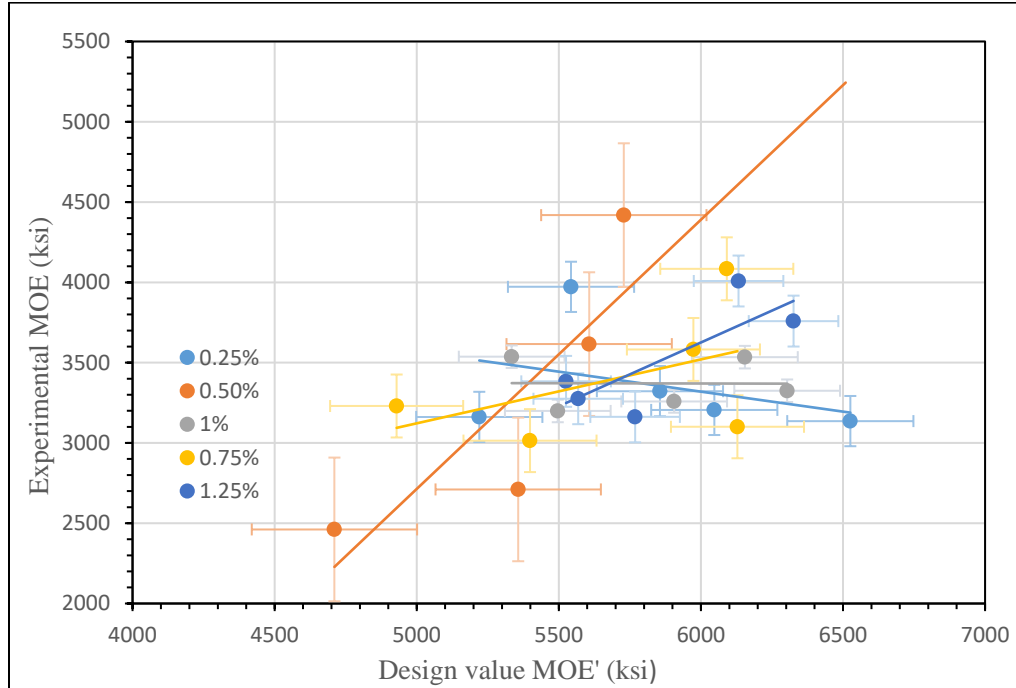
Figure 4.15: Relationship between experimental MOE and design value MOE' isolating
steel fiber effect

Figure 4:16 represents the relation between experimental and design value
modulus of elasticity isolating temperature condition. The linear relations are listed from
4.20 to 4.24.

$$\text{MOE(ksi)} = 0.3087\text{MOE}' + 1857.3 \qquad T = -25^0C \quad (4.20)$$

$$\text{MOE(ksi)} = -0.0536\text{MOE}' + 3728.3 \qquad T = -5^0C \quad (4.21)$$

$$\text{MOE(ksi)} = 0.4425\text{MOE}' + 853.39 \qquad T = 15^0C \quad (4.22)$$

$$\text{MOE(ksi)} = 0.4084\text{MOE}' + 7018.5 \qquad T = 35^0C \quad (4.23)$$

$$\text{MOE(ksi)} = 0.6942\text{MOE}' + 7018.5 \qquad T = 55^0C \quad (4.24)$$
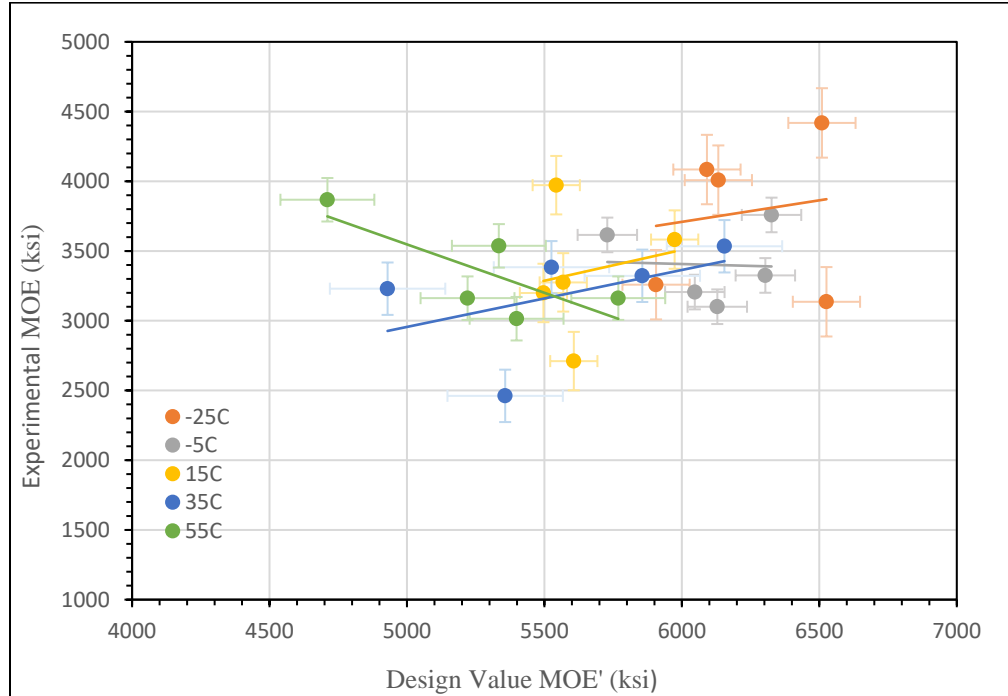
Figure 4.16: Relationship between experimental MOE and design value MOE' isolating temperature effect

The linear regressions are found to be the best fit for the data points in the plots. As presented, the plot is quite scattered to predict an effective relationship. Although, an increasing trend has been observed for experimental MOE with the rise in design value MOE′ except at higher temperature and low steel fiber volume. Values that fall below the design value of MOE are problematic as deflection and serviceability for beams constructed of this material would be under-predicted.

4.5   Summary

The test results and overall observations are summarized in this section. The section is in turn divided into three subsections illustrating compressive strength, flexural strength and toughness, and modulus of elasticity.

4.5.1   Compressive Strength

Subzero temperature improved compressive strength to the maximum. Among all the temperature conditions -25^0C showed an overall higher strength. At each of the temperature level the strength increased gradually, although there are some reductions at an increasing rate. The improvements in compressive strength are 57.5%, 51.7%, 75.8%, 12.4% and 29.1% respectively from 0.25%-1.25% steel volume level. At -25^0C the specimens were kept in the freezing chamber longer than the designed time. Therefore, a subtle difference in the results at this temperature has been noticed throughout the experiments. Steel fibers improved compressive strength in general with a high standard deviation compared to previous study (Sarfin 2019). Compressive strength also has improved with the addition of higher amount of steel fiber. The plots are somewhat scattered; therefore, no specific relationship could be found between the steel fiber amount and compressive strength.

4.5.2   Flexural Strength and Toughness

Overall, flexural strength showed an increase in both directions from 15^0C up to $\pm20^0$C. Again, a reduction has been observed at further $\pm20^0$C in both elevated and subzero temperatures. The cementitious matrix appeared to dominate the flexural strength at temperature level. The effect of steel fiber is indistinct among all the specimen groups. A slight improvement in the strength has been noticed in general at higher steel fiber volume. The steel fiber content up to 1.25% does not seem much beneficial. An apparent contribution of steel fiber has been noticed in the failure pattern. Most of the specimens have showed failure in a ductile manner yet there are some dissimilarities. Due to effect

of fiber bridging the strain hardening regions are visible, which demonstrates a fair energy absorption capacity of the specimens. However, at elevated temperatures the fiber bridging behavior almost disappeared. Thus, an improved toughness has been noticed because of concrete matrix strength mostly. At 0.5%, 0.75% and 1.00% the toughness seems to be the maximum, yet this event is not clear enough to come into a conclusion.

4.5.3 Static Modulus of Elasticity

Static modulus of elasticity (MOE) of the specimens are sought from 40% load values of the compressive strengths at failure. At lower temperature static modulus of elasticity mostly seems to improve except some anomalies. Effect of steel fibers are also conspicuous in a subtle manner. In more than 50% cases MOE increased at higher steel fiber volume. It is found in the literature that compressive strength highly depends on the shape of the specimens (Vitek et al. 2013). Hence, point to be noted, the specimen dimensions of compressive strength test and MOE test are not the same. Therefore, load value from different dimensioned specimen could affect the test results.

Linear relationships are found based on regression between MOE and square root of compressive strength and design value and experimental MOE. These relations can predict modulus of elasticity.

CHAPTER 5

CONCLUSION AND FUTURE DIRECTION

5.1   Conclusion

This section discusses the results from laboratory experiments and the objectives of this research. The section is divided into two parts. The first part presents the conclusions from the experimental results. And the second part provides the future direction of this research work.

The results obtained from experiments are evaluated, analyzed and trends are assessed in order to realize the mechanical properties. The main objective of this experimental study is to understand the impact of ambient temperature and steel fiber volume on the mechanical properties of UHPC. Most of the tests results are complementary with the existing literature.

Compressive strength seems to be affected clearly by the temperature at service level. From -25^0C to 55^0C temperature range, which is typically observed in the atmosphere, the micro structure of cementitious matrix experiences several chemical and physical phases. The results show a visible variation in compressive strengths probably due to the hydration reaction, development of porosity, formation of calcium hydroxide $(Ca(OH)_2)$ and calcium silicate hydrates (C-H-S) compounds. Based on the observation, compressive strength increases at below zero temperature. The maximum compressive strength is found 21.3 ksi at 0.75% steel fiber volume. Steel fiber seems to improve compressive strength slightly with an increased fiber content. The increment is recorded

10%-22% in spite of some anomalies. In addition, a clear improvement is noticed for specimens with steel fiber compared to without steel fiber.

Temperature effect of flexural strength corresponds to the behavior of cementitious matrix under the variation of temperature. This phenomenon depicts that the contribution of cementitious matrix is higher than fibers itself. Although steel fibers work better in flexure, the effect of steel fiber in the flexural strength is subtle. The plot is scattered with a slight improvement at higher steel fiber volume. In some of the specimens (NB at 55^0C) the load deflection curve barely exhibited the fiber bridging characteristic, which eventually resulted lower ultimate strength. The action of fibers is not very clear. Possibly it is due to the incongruous response of the concrete and steel fiber under different temperatures. The case is nearly the same for flexural toughness. At elevated temperatures the action of steel fiber is unclear.

Static modulus of elasticity seems to improve in general at below zero temperature and at higher steel fiber volume. Both agree with the existing literature. The positive effect of steel fiber confirms the fiber confinement in the matrix. However, the experimentally obtained modulus is lower than design value. In many of the cases it is nearly half. Lastly, correlations between laboratory obtained test results, square root of compressive strength, and modulus of elasticity from ACI equation are developed.

5.2   Future Direction

The goal of this research work is to develop sustainable UHPC at atmospheric service temperature condition. Especially, it aims to analyze the mechanical properties

and the contribution of steel fiber content at material level. Keeping the goal in mind, this work is an attempt to make UHPC under laboratory condition.

After assessing the experimental results, it is clear that a better understanding of steel fiber's contribution warrants further research. Throughout the experiments the action of steel fibers is seldom, especially in three-point bending test. Pull out of fibers becomes easy when the fiber matrix bond is not strong enough to resist the stress transfer. Hence, a microscopic analysis of the matrix interface felt necessary. Also, the physical property of steel fiber plays a vital role in the matrix bond. The steel fiber has been used in this research work is 0.5 inch long double helix micro fibers. The contribution of this micro fiber is discernable in the load deflection curve for most of the specimens (e.g. except at elevated temperature). Yet, understanding the contribution of micro fibers is a requisite to realize the reason behind the insensitivity of steel fiber at elevated temperature, especially in the case of toughness. Additionally, the flexural strength and toughness mostly depends on the fiber matrix bond which is in turn dependent on the fiber shape, length, and aspect ratio. Many researchers successfully have shown the effect of physical properties of steel fiber on pull out behavior and eventually the toughness (Li et al. 2020)(Wu et al. 2018). Hence, an incorporation of other fiber types might help to better understand the situation. At point of failure, it is conspicuous that all the fibers did not participate to sustain load due to its bizarre orientation. A detailed alignment can probably minimize this effect (Huang et al. 2021). Afterall, an investigation incorporating higher volume content of steel fibers can provide a better picture (Wang et al. 2017). Because, it is clear from the results that up to 1.25% fiber volume does not affect the

mechanical properties to a good extent. In future work, these reasonings can be addressed.

UHPC is consists of low w/b ratio. Therefore, in order to achieve desired workability, the dosage of superplasticizer goes higher. It is reported earlier that higher superplasticizer is prone to entrap air bubbles (Wang et al. 2019). Therefore, the dosage of superplasticizer can be a concern. This experimental work employed high dosage of superplasticizer than designed value to achieve a workable concrete. Hence, it is felt that a better optimization at material level can enlighten the future work. However, to confirm this hypothesis a microscopic analysis is necessary.

This work is limited to the service-temperature. Therefore, to fully understand the effect of temperature on UHPC a broad range of temperature exposure is significant. In micro structural level, compounds generated from hydration reaction effects the mechanical properties remarkably. Understanding the chemical reactions and their consequences is paramount to make operational UHPC. An investigation of durability, such as, freeze thaw test and chloride ion test can be performed to justify the material's longevity. Along with temperature, the inclusion of humidity, ecological impact can enrich this research from global pint of view. The large-scale experiments at structural level and numerical analysis along with finite element analysis can be a significant future work. Thus, major relations and equations can be developed that can impart a great contribution to improve the existing code.

REFERENCES

Abbas, S., Soliman, A. M., and Nehdi, M. L. (2015). "Exploring mechanical and durability properties of ultra-high performance concrete incorporating various steel fiber lengths and dosages." *Construction and Building Materials*, Elsevier Ltd, 75, 429–441.

ACI Committee. (2005). "Building code requirements for structural concrete (ACI 318-05) and commentary (ACI 318R-05)." *American Concrete Institute*.

Ahmad, S., Rasul, M., Adekunle, S. K., Al-Dulaijan, S. U., Maslehuddin, M., and Ali, S. I. (2019). "Mechanical properties of steel fiber-reinforced UHPC mixtures exposed to elevated temperature: Effects of exposure duration and fiber content." *Composites Part B: Engineering*, Elsevier, 168, 291–301.

Alkaysi, M., El-Tawil, S., Liu, Z., & Hansen, W. (2016). "Effects of silica powder and cement type on durability of ultra high performance concrete (UHPC)." *Cement and Concrete Composites*, 66, 47-56.

ASTM. (2016). "ASTM C150-16, Standard Specification for Portland Cement." ASTM International, West Conshohocken, PA.

ASTM. (2015). "ASTM C39-15, Standard Test Method for Compressive Strength of Cylindrical Concrete Specimens." ASTM International, West Conshohocken, PA.

ASTM. (2013). "ASTM C42-13, Standard Test Method for Obtaining and Testing Drilled Cores and Sawed Beams of Concrete." ASTM International, West Conshohocken, PA.

ASTM. (2015). "ASTM C78-15, Standard Test Method for Flexural Strength of Concrete

(Using Simple Beam with Third-Point Loading)." ASTM International, West Conshohocken, PA.

ASTM. (2015). "ASTM C 1240-15, Standard Specification for Silica Fume Used in Cementitious Mixtures." ASTM International, West Conshohocken, PA.

ASTM. (2017). "ASTM C1856 / C1856M - 17, Standard Practice for Fabricating and Testing Specimens of Ultra-High Performance Concrete." ASTM International, West Conshohocken, PA.

ASTM. (2019). "ASTM C192 / C192M - 19, Standard Practice for Making and Curing Concrete Test Specimens in the Laboratory." ASTM International, West Conshohocken, PA.

ASTM. (2014). "ASTM C469 / C469M - 14, Standard Test Method for Static Elasticity and Poisson's Ratio of Concrete in compression." ASTM International, West Conshohocken, PA.

ASTM. (2013). "ASTM C174 / C174M - 13, Standard Test Method for Measuring Thickness of Concrete Elements Using Drilled Concrete Cores." ASTM International, West Conshohocken, PA.

ASTM. (2017). "ASTM C494 / C494M - 17, Standard Specification for Chemical Admixtures for Concrete." ASTM International, West Conshohocken, PA.

ASTM. (2015). "ASTM C617 / C617M - 15, Standard Practice for Capping Cylindrical Concrete Specimens." ASTM International, West Conshohocken, PA.

ASTM. (1997). "ASTM C1018 / C1018M - 97, Standard Test Method for Flexural Toughness and First-Crack Strength of Fiber-Reinforced Concrete (Using Beam

with Third-Point Loading).” ASTM International, West Conshohocken, PA

Berry, M., Johnson, J., and McDevitt, K. (2017). “Effect of cold temperatures on the behavior and ultimate capacity of GFRP-reinforced concrete beams.” *Cold Regions Science and Technology*, Elsevier B.V., 136, 9–16.

Cao, Y., & Detwiler, R. J. (1995). “Backscattered electron imaging of cement pastes cured at elevated temperatures.” *Cement and Concrete Research*, 25(3), 627-638.

F.de Larrard, T. S. (1994). “Optimization of ultra-high-performance concrete by the use of a packing model.” *Cement and Concrete Research*, 24(6), 997–1009.

Gao, J., Sun, W., & Morino, K. (1997). “Mechanical properties of steel fiber-reinforced, high-strength, lightweight concrete.” *Cement and Concrete Composites*, 19(4), 307-313.

Graybeal, B. A. (2007). “Compressive Behavior of Ultra-High-Performance Fiber-Reinforced Concrete.” 146(104), 2007.

Graybeal, B. (2011). “Ultra-High Performance Concrete (FHWA-HRT-11-038).” *Federal Highway Administration,* Washington, DC.

Graybeal, B. a., and Stone, B. (2012). “TECHBRIEF Compression Response of a Rapid-Strengthening Ultra-High Performance Concrete Formulation.” (September), 1–6.

Graybeal, B., and Tanesi, J. (2008). “A cementitious long-life wearing course to reduce frequency of maintenance works on high-traffic roads.” *Transport Research Arena Europe 2008*, 1561(February), 454–461.

Hajar, Z., Resplendino, J., Lecointre, D., Petitjean, J., and Simon, A. (2004). “Ultra-high-performance concretes: First recommendations and examples of application.”

Proceedings of the fib Symposium 2004 - Concrete Structures: The Challenge of Creativity.

He, B., Zhu, X., Ren, Q., and Jiang, Z. (2020). "Effects of fibers on flexural strength of ultra-high-performance concrete subjected to cryogenic attack." *Construction and Building Materials*, Elsevier Ltd, 265, 120323.

Huang, H., Gao, X., and Khayat, K. H. (2021). "Contribution of fiber alignment on flexural properties of UHPC and prediction using the Composite Theory." *Cement and Concrete Composites*, Elsevier Ltd, 118(February), 103971.

Huang, H., Gao, X., Li, L., and Wang, H. (2018). "Improvement effect of steel fiber orientation control on mechanical performance of UHPC." *Construction and Building Materials*, Elsevier Ltd, 188, 709–721.

Husem, M. (2006). "The effects of high temperature on compressive and flexural strengths of ordinary and high-performance concrete." *Fire Safety Journal*, 41(2), 155–163.

Jianming Gao, Wei Sun, K. M. (1997). "Mechanical Properties of Steel Fiber Reinforced High-Strength Lightweight Concrete." *Jianzhu Cailiao Xuebao/Journal of Building Materials*, 24(1), 63–70.

Kaleta-Jurowska, A., and Jurowski, K. (2020). "The influence of ambient temperature on high performance concrete properties." *Materials*, 13(20), 1–16.

Kim, S., Kim, M. J., Yoon, H., and Yoo, D. Y. (2018). "Effect of cryogenic temperature on the flexural and cracking behaviors of ultra-high-performance fiber-reinforced concrete." *Cryogenics*, Elsevier, 93(June), 75–85.

Klamer, E. L. (2009). "Influence of temperature on concrete beams strengthened in flexure with CFRP." *Eindhoven, Netherlands: Eindhoven University of Technology*.

Krstulovic-Opara, N. (2007). "Liquefied natural gas storage: Material behavior of concrete at cryogenic temperatures." *ACI materials journal*, *104(3), 297*.

Lee, M. G., Wang, Y. C., and Chiu, C. Te. (2007). "A preliminary study of reactive powder concrete as a new repair material." *Construction and Building Materials*, 21(1), 182–189.

Li, Y., Yang, E. H., and Tan, K. H. (2020). "Flexural behavior of ultra-high performance hybrid fiber reinforced concrete at the ambient and elevated temperature." *Construction and Building Materials*, 250.

Lothenbach, B., Winnefeld, F., Alder, C., Wieland, E., and Lunk, P. (2007). "Effect of temperature on the pore solution, microstructure and hydration products of Portland cement pastes." *Cement and Concrete Research*, 37(4), 483–491.

Ma, Q., Guo, R., Zhao, Z., Lin, Z., and He, K. (2015). "Mechanical properties of concrete at high temperature-A review." *Construction and Building Materials*, Elsevier Ltd, 93, 371–383.

Pierre Richard, M. C. (1995). "Composition of reactive powder concretes." *Cement and Concrete Research*, 25(7), 1501–1511.

Poon, C. S., Shui, Z. H., and Lam, L. (2004). "Compressive behavior of fiber reinforced high-performance concrete subjected to elevated temperatures." *Cement and Concrete Research*, 34(12), 2215–2222.

Rabbat, B. G., and Russell, H. G. (1982). "Optimized Sections for Precast Prestressed

Bridge Girders." *Journal - Prestressed Concrete Institute*, 27(4), 88–104.

Raza, S. S., Qureshi, L. A., Ali, B., Raza, A., and Khan, M. M. (2021). "Effect of different fibers (steel fibers, glass fibers, and carbon fibers) on mechanical properties of reactive powder concrete." *Structural Concrete*, 22(1), 334–346.

Richard, P., & Cheyrezy, M. (1995). "Composition of reactive powder concretes." *Cement and concrete research*, 25(7), 1501-1511.

Saad, M., Abo-El-Enein, S. A., Hanna, G. B., & Kotkata, M. F. (1996). "Effect of temperature on physical and mechanical properties of concrete containing silica fume." *Cement and concrete research*, 26(5), 669-675.

Sarfin, M.A.A. (2019). "Parametric Study of Mixture Component Contributions to Compressive Strength and Impact Energy Absorption Capacity of a High Strength Cementitious Mix with No Coarse Aggregate." *Utah State University*.

Schmidt, M., and Fehling, E. (2005). "Ultra-high-performance concrete: Research, development and application in Europe." *Seventh International Symposium on the Utilization of High Strength/High-Performance Concrete*, 51–78.

Shi, C., Wu, Z., Xiao, J., Wang, D., Huang, Z., and Fang, Z. (2015). "A review on ultra high performance concrete: Part I. Raw materials and mixture design." *Construction and Building Materials*, Elsevier Ltd, 101, 741–751.

Shoukry, S. N., William, G. W., Downie, B., and Riad, M. Y. (2011). "Effect of moisture and temperature on the mechanical properties of concrete." *Construction and Building Materials*, Elsevier Ltd, 25(2), 688–696.

Soliman, N. A., and Tagnit-Hamou, A. (2017). "Using particle packing and statistical

approach to optimize eco-efficient ultra-high-performance concrete." *ACI Materials Journal*, 114(6), 847–858.

Song, P. S., and Hwang, S. (2004). "Mechanical properties of high-strength steel fiber-reinforced concrete." *Construction and Building Materials*, 18(9), 669–673.

Tai, Y. S., and El-Tawil, S. (2019). "Computational investigation of twisted fiber pullout from ultra-high performance concrete." *Construction and Building Materials*, Elsevier Ltd, 222, 229–242.

Thomas, R. J., Bedke, C., and Sorensen, A. (2017). "Dynamic Shear Energy Absorption of Ultra-High Performance Concrete." *World Academy of Science, Engineering and Technology, International Journal of Civil, Environmental, Structural, Construction and Architectural Engineering*, 11(3), 286–291.

Thomas, R. J., and Sorensen, A. D. (2017). "Review of strain rate effects for UHPC in tension." *Construction and Building Materials*, 153, 846–856.

Vitek, J. L., Coufal, R., and Čítek, D. (2013). "UHPC - Development and testing on structural elements." *Procedia Engineering*, 65, 218–223.

Wang, R., and Gao, X. (2016). "Relationship between flowability, entrapped air content and strength of UHPC mixtures containing different dosage of steel fiber." *Applied Sciences (Switzerland)*, 6(8).

Wang, R., Gao, X., Huang, H., and Han, G. (2017). "Influence of rheological properties of cement mortar on steel fiber distribution in UHPC." *Construction and Building Materials*, Elsevier Ltd, 144, 65–73.

Wang, X., Yu, R., Song, Q., Shui, Z., Liu, Z., Wu, S., and Hou, D. (2019). "Optimized

design of ultra-high performance concrete (UHPC) with a high wet packing density." *Cement and Concrete Research*, Elsevier, 126(June 2018), 105921.

Wiemer, N., Wetzel, A., Schleiting, M., Krooß, P., Vollmer, M., Niendorf, T., Böhm, S., and Middendorf, B. (2020). "Effect of fibre material and fibre roughness on the pullout behaviour of metallic micro fibres embedded in UHPC." *Materials*, 13(14), 1–21.

Wu, Z., Khayat, K. H., and Shi, C. (2018). "How do fiber shape and matrix composition affect fiber pullout behavior and flexural properties of UHPC?" *Cement and Concrete Composites*, Elsevier, 90(October 2016), 193–201.

Wu, Z., Shi, C., He, W., and Wang, D. (2017). "Static and dynamic compressive properties of ultra-high performance concrete (UHPC) with hybrid steel fiber reinforcements." *Cement and Concrete Composites*, Elsevier Ltd, 79, 148–157.

Wu, Z., Shi, C., He, W., and Wu, L. (2016). "Effects of steel fiber content and shape on mechanical properties of ultra high performance concrete." *Construction and Building Materials*, Elsevier Ltd, 103, 8–14.

Yang, I. H., Joh, C., and Kim, B. S. (2011). "Flexural strength of ultra high strength concrete beams reinforced with steel fibers." *Procedia Engineering*, Elsevier B.V., 14, 793–796.

Yang, I. H., and Park, J. (2019). "Mechanical and Thermal Properties of UHPC Exposed to High-Temperature Thermal Cycling." *Advances in Materials Science and Engineering*, 2019.

Yoo, D. Y., Lee, J. H., and Yoon, Y. S. (2013). "Effect of fiber content on mechanical

and fracture properties of ultra high performance fiber reinforced cementitious composites." *Composite Structures*, Elsevier Ltd, 106, 742–753.

Zhang, G., Yang, Y., Yang, H., and Li, H. (2020a). "Calcium sulphoaluminate cement used as mineral accelerator to improve the property of Portland cement at sub-zero temperature." *Cement and Concrete Composites*, Elsevier Ltd, 106(August 2018), 103452.

Zhang, Y., Zhu, Y., Qu, S., Kumar, A., and Shao, X. (2020b). "Improvement of flexural and tensile strength of layered-casting UHPC with aligned steel fibers." *Construction and Building Materials*, Elsevier Ltd, 251, 118893.

APPENDICES

APPENDIX A. COMPRESSIVE STRENGTH RESULTS

Group 1 (-25^{0}C)				
Steel fiber (%)	Specimen No.	Average Length (inch)	Average Diameter (inch)	Compressive strength (psi)
0.25	C1-11	5.870	2.993	17907
	C1-12	5.883	3.020	17636
	C1-13	5.870	3.010	19839
	C1-14	5.897	2.993	19082
	C1-15	5.853	3.000	14221
0.5	C1-21	5.913	3.030	15254
	C1-22	5.937	3.020	26163
	C1-23	5.900	3.020	16470
	C1-24	5.777	3.020	13844
	C1-25	7.277	3.007	16508
0.75	C1-31	5.893	3.030	16212
	C1-32	5.933	3.033	14846
	C1-33	5.917	3.023	8853
	C1-34	5.930	2.990	20292
	C1-35	5.927	3.003	17059
1	C1-41	5.940	3.000	13263
	C1-42	5.910	3.003	16563
	C1-43	5.907	3.010	12853
	C1-44	5.863	3.010	18697
	C1-45	5.930	3.007	11261
1.25	C1-51	5.903	3.013	11777
	C1-52	5.937	2.993	18160
	C1-53	5.870	3.007	16133
	C1-54	5.913	2.997	17089
	C1-55	5.923	3.010	15159

Group 2 (-5^{0}C)				
Steel fiber (%)	Specimen No.	Average Length (inch)	Average Diameter (inch)	Compressive strength (psi)
0.25	C2-11	5.993	3.023	13339
	C2-12	6.003	2.990	12006
	C2-13	5.967	2.993	17746
	C2-14	5.993	2.987	13685
	C2-15	5.993	3.000	19374
0.5	C2-21	5.993	3.017	16617
	C2-22	6.017	3.017	13441
	C2-23	6.000	3.017	13624
	C2-24	5.967	3.017	10633
	C2-25	5.980	3.030	14028
0.75	C2-31	5.960	3.013	13764
	C2-32	5.987	2.993	8270
	C2-33	5.813	2.990	24930
	C2-34	5.990	3.003	12720
	C2-35	6.013	2.993	18535
1	C2-41	5.990	2.993	14707
	C2-42	6.013	3.023	17200
	C2-43	5.957	3.017	17511
	C2-44	5.990	2.987	16122
	C2-45	5.973	3.013	17206
1.25	C2-51	5.967	2.993	20377
	C2-52	5.987	2.997	22525
	C2-53	5.983	3.000	8433
	C2-54	5.960	3.013	14812
	C2-55	5.943	2.997	17190

Group 3 (15^{0}C)				
Steel fiber (%)	Specimen No.	Average Length (inch)	Average Diameter (inch)	Compressive strength (psi)
0.25	C3-11	6.003	3.000	14456
	C3-12	5.927	3.000	14357
	C3-13	5.940	3.010	11008
	C3-14	6.010	3.003	16201
	C3-15	5.977	3.003	7960
0.5	C3-21	6.003	3.020	9988
	C3-22	3.013	5.727	18622
	C3-23	5.987	2.987	10413
	C3-24	5.950	3.013	11173
	C3-25	5.983	2.990	15269
0.75	C3-31	5.960	3.010	11920
	C3-32	5.977	2.980	9894
	C3-33	5.973	2.970	15198
	C3-34	6.000	2.990	23348
	C3-35	6.020	3.010	13953
1	C3-41	5.923	3.027	9425
	C3-42	5.940	3.023	13105
	C3-43	5.970	2.980	11883
	C3-44	5.977	2.987	15824
	C3-45	5.990	2.987	12674
1.25	C3-51	5.970	3.003	12670
	C3-52	5.940	3.017	13718
	C3-53	5.957	3.007	15818
	C3-54	6.000	3.000	11710
	C3-55	5.983	3.000	10653

Group 4 (35^0C)				
Steel fiber (%)	Specimen No.	Average Length (inch)	Average Diameter (inch)	Compressive strength (psi)
0.25	C4-11	5.953	3.013	15386
	C4-12	5.940	3.020	12971
	C4-13	5.983	3.020	9315
	C4-14	5.977	2.993	23683
	C4-15	5.967	2.983	10057
0.5	C4-21	5.963	3.003	11619
	C4-22	5.953	3.040	9205
	C4-23	5.923	3.013	19604
	C4-24	5.997	3.000	12641
	C4-25	5.950	2.987	6695
0.75	C4-31	5.953	3.007	11679
	C4-32	5.967	3.007	9760
	C4-33	5.947	2.987	11242
	C4-34	5.997	2.973	9307
	C4-35	5.963	2.983	8612
1	C4-36	5.963	3.043	14643
	C4-37	5.963	3.010	19977
	C4-38	5.950	3.013	15476
	C4-39	5.940	2.983	17351
	C4-40	6.007	2.997	11441
1.25	C4-51	5.930	3.003	11598
	C4-52	5.997	2.993	10889
	C4-53	5.990	3.023	12684
	C4-54	5.963	3.003	16406
	C4-55	5.930	2.983	12006

Group 5 (55^{0}C)				
Steel fiber (%)	Specimen No.	Average Length (inch)	Average Diameter (inch)	Compressive strength (psi)
0.25	C5-11	5.963	2.993	16124
	C5-12	5.997	3.000	9396
	C5-13	5.987	3.007	15234
	C5-14	6.003	3.013	6718
	C5-15	5.910	2.963	9275
0.5	C5-21	5.977	3.013	9343
	C5-22	6.007	3.017	11520
	C5-23	6.000	2.993	8394
	C5-24	5.963	3.007	9720
	C5-25	5.963	3.007	7228
0.75	C5-31	6.000	3.013	16747
	C5-32	6.000	3.010	9661
	C5-33	5.967	3.020	14054
	C5-34	5.987	3.023	9946
	C5-35	5.947	3.010	10286
1	C5-36	6.007	3.023	12921
	C5-37	5.997	3.013	7860
	C5-38	5.983	3.007	8809
	C5-39	5.953	3.000	18323
	C5-40	5.993	3.010	11340
1.25	C5-51	5.980	3.020	15591
	C5-52	5.993	3.003	12724
	C5-53	5.957	2.983	13398
	C5-54	6.010	3.000	14613
	C5-55	5.930	2.990	12969

APPENDIX B. FLEXURAL STRENGTH RESULTS

Group 1 (-25^{0}C)					
Steel Fiber (%)	Specimen No.	Average Length (inch)	Average Width (inch)	Average Depth (inch)	Flexural Strength (psi)
	B0-11	12.125	3.040	3.047	473
0.25	B0-12	12.000	3.010	3.323	528
	B0-13	12.000	3.027	3.040	384
	B0-21	12.083	3.040	3.007	311
0.5	B0-22	12.167	3.080	3.073	336
	B0-23	12.042	3.020	3.020	234
	B0-31	12.083	3.067	2.993	219
0.75	B0-32	12.083	3.037	2.980	279
	B0-33	12.083	3.067	3.033	311
	B0-41	12.125	3.097	3.043	340
1	B0-42	12.083	3.020	3.077	-
	B0-43	12.083	3.087	2.993	158
	B0-51	12.125	3.050	3.013	348
1.25	B0-52	12.125	3.043	3.023	295
	B0-53	12.083	3.073	3.077	272
Group 2 (-5^{0}C)					
Steel Fiber (%)	Specimen No.	Average Length (inch)	Average Width (inch)	Average Depth (inch)	Flexural Strength (psi)
	B2-11	12.042	3.033	3.013	147
0.25	B2-12	12.000	3.047	3.080	362
	B2-13	12.000	3.013	3.100	420
	B2-21	12.083	3.013	3.033	363
0.5	B2-22	12.042	2.937	3.083	263
	B2-23	12.042	3.020	3.020	370
	B2-31	12.042	2.953	3.003	304
0.75	B2-32	12.042	3.013	3.063	263
	B2-33	12.125	2.997	3.073	311
	B2-41	12.083	2.993	2.987	276
1	B2-42	12.083	2.977	3.007	459
	B2-43	12.042	3.053	3.013	284
	B2-51	12.083	3.047	2.983	305
1.25	B2-52	12.042	2.973	2.997	298
	B2-53	12.042	3.067	3.077	826

Group 3 (15^{0}C)					
Steel Fiber (%)	Specimen No.	Average Length (inch)	Average Width (inch)	Average Depth (inch)	Flexural Strength (psi)
0.25	B3-11	12.000	3.107	2.997	264
	B3-12	12.000	3.010	2.990	289
	B3-13	12.000	3.093	3.087	126
0.5	B3-21	12.125	2.990	3.017	283
	B3-22	11.958	2.990	100.983	221
	B3-23	12.000	3.013	3.030	279
0.75	B3-31	12.083	3.003	2.973	186
	B3-32	12.125	3.010	3.050	260
	B3-33	12.083	2.983	3.020	329
1	B3-41	12.167	2.890	2.990	244
	B3-42	12.083	3.017	3.010	265
	B3-43	12.083	2.983	2.990	245
1.25	B3-51	12.083	3.003	3.097	383
	B3-52	12.083	3.033	3.053	-
	B3-53	12.083	2.983	2.990	336
Group 4 (35^{0}C)					
Steel Fiber (%)	Specimen No.	Average Length (inch)	Average Width (inch)	Average Depth (inch)	Flexural Strength (psi)
0.25	B4-11	12.042	2.953	2.960	266
	B4-12	12.000	3.013	2.983	403
	B4-13	11.958	3.027	2.963	328
0.5	B4-21	12.125	3.080	3.013	515
	B4-22	12.000	2.997	2.993	301
	B4-23	12.000	3.017	2.967	378
0.75	B0-31	12.083	3.100	3.013	320
	B0-32	12.042	3.083	2.983	343
	B0-33	12.125	3.167	3.043	305
1	B0-41	12.125	3.057	3.020	338
	B0-42	12.167	2.993	3.020	341
	B0-43	12.125	3.077	2.987	405
1.25	B0-51	12.000	2.963	2.970	283
	B0-52	12.083	3.033	3.020	281
	B0-53	12.083	2.977	3.100	284

Group 5 (55^{0}C)					
Steel Fiber (%)	Specimen No.	Average Length (inch)	Average Width (inch)	Average Depth (inch)	Flexural Strength (psi)
0.25	B5-11	12.000	3.060	2.993	341
	B5-12	11.958	3.023	3.033	137
	B5-13	12.083	3.067	2.957	603
0.5	B5-21	12.083	3.060	3.013	512
	B5-22	12.000	3.053	2.993	360
	B5-23	12.042	3.043	2.997	467
0.75	B5-31	12.083	3.053	3.050	346
	B5-32	12.083	3.067	2.983	538
	B5-33	12.042	3.060	3.060	298
1	B5-41	12.125	3.007	3.003	344
	B5-42	12.042	3.083	3.003	370
	B5-43	12.042	3.070	3.037	378
1.25	B5-51	12.000	3.090	2.980	291
	B5-52	12.042	3.083	3.100	727
	B5-53	12.083	3.087	3.047	268

APPENDIX C. FLEXURAL TOUGHNESS RESULTS

Group 1 (-25^{0}C)				
Steel Fiber (%)	Specimen No.	First Crack Strength (psi)	Ultimate Strength (psi)	Toughness (lb-inch)	Area under Load Deflection Curve (lb-inch)
0.25	B1-11	242	1679	0.79	142.48
	B1-12	221	1675	0.32	144.71
	B1-13	224	2167	0.36	220.34
0.5	B1-21	229	1430	0.05	116.47
	B1-22	244	1956	0.45	182.85
	B1-23	231	2052	0.48	204.44
0.75	B1-31	216	725	0.28	43.26
	B1-32	428	2179	7.76	281.78
	B1-33	208	1390	0.10	107.69
1	B1-41	1410	2045	94.07	109.80
	B1-42	690	2225	16.87	270.79
	B1-43	377	2070	3.51	218.51
1.25	B1-51	253	1465	1.18	163.04
	B1-52	278	1451	1.41	164.52
	B1-53	357	1308	2.26	172.32
Group 2 (-5^{0}C)				
Steel Fiber (%)	Specimen No.	First Crack Strength (psi)	Ultimate Strength (psi)	Toughness (lb-inch)	Area under Load Deflection Curve (lb-inch)
0.25	B2-11	216	719	0.11	39.46
	B2-12	220	1590	0.34	128.39
	B2-13	207	1331	0.14	87.97
0.5	B2-21	365	1524	5.09	124.56
	B2-22	1247	1247	71.13	81.42
	B2-23	1755	1755	139.55	154.13
0.75	B2-31	1507	1507	114.75	164.18
	B2-32	1207	1207	63.28	72.17
	B2-33	210	1488	0.10	115.64
1	B2-41	232	1352	0.54	131.51
	B2-42	212	1465	0.10	108.30
	B2-43	1284	1285	75.09	90.78
1.25	B2-51	213	1484	0.67	139.48
	B2-52	281	1421	1.28	129.21

	B2-53	1538	1735	108.93	160.00
			Group 3 (15^0C)		
Steel Fiber (%)	Specimen No.	First Crack Strength (psi)	Ultimate Strength (psi)	Toughness (lb-inch)	Area under Load Deflection Curve (lb-inch)
0.25	B3-11	225	1127	0.43	68.96
	B3-12	227	1096	18.79	57.95
	B3-13	297	608	4.16	36.92
0.5	B3-21	260	1340	1.58	155.61
	B3-22	240	1033	0.51	86.91
	B3-23	293	1174	5.09	121.68
0.75	B3-31	828	869	31.48	99.57
	B3-32	307	1288	1.57	153.54
	B3-33	265	1139	1.77	81.49
1	B3-41	1132	1213	57.59	142.20
	B3-42	253	1192	0.63	135.16
	B3-43	684	1130	15.98	91.93
1.25	B3-51	277	1713	1.00	163.31
	B3-52	305	305	2.14	10.56
	B3-53	310	1549	5.61	119.04
			Group 4 (35^0C)		
Steel Fiber (%)	Specimen No.	First Crack Strength (psi)	Ultimate Strength (psi)	Toughness (lb-inch)	Area under Load Deflection Curve (lb-inch)
0.25	B4-11	868	1315	30.22	81.57
	B4-12	439	1554	7.38	125.46
	B4-13	1449	1449	96.85	105.69
0.5	B4-21	614	1169	13.08	62.60
	B4-22	1450	1451	94.12	107.66
	B4-23	1494	1495	102.15	112.94
0.75	B0-31	370	1563	3.35	123.32
	B0-32	1448	1448	100.23	117.27
	B0-33	240	1510	0.34	105.73
1	B0-41	215	1604	0.21	159.31
	B0-42	1550	1552	113.93	132.50
	B0-43	230	1594	0.28	150.66
1.25	B0-51	438	1377	4.65	130.70
	B0-52	364	1315	2.99	133.57
	B0-53	643	1377	16.01	121.67

Group 5 (55^{0}C)				
Steel Fiber (%)	Specimen No.	First Crack Strength (psi)	Ultimate Strength (psi)	Toughness (lb-inch)	Area under Load Deflection Curve (lb-inch)
0.25	B5-11	1530	0.136	105.52	114.65
	B5-12	670	0.0565	17.44	57.62
	B5-13	770	0.0495	21.58	94.86
0.5	B5-21	255	0.0148	0.50	105.87
	B5-22	1419	0.1148	87.64	95.93
	B5-23	1278	0.1025	70.53	76.75
0.75	B5-31	1560	0.1672	107.44	126.45
	B5-32	1541	0.1372	109.25	127.76
	B5-33	1465	0.124	92.97	145.73
1	B5-41	242	0.0165	0.51	160.20
	B5-42	226	0.0085	0.22	104.94
	B5-43	1475	0.1412	107.33	121.08
1.25	B5-51	207	0.0342	0.10	152.67
	B5-52	326	0.015	1.57	140.10
	B5-53	361	0.0185	2.94	114.80

APPENDIX D. MODULUS OF ELASTICITY RESULTS

Group 1 (-25^{0}C)							
Steel Fiber (%)	Specimen No.	% Load	Average Stress (ksi)	Average Strain (in/in)	Parameters		Average MOE (ksi)
	M1-11	10	0.993180	0.0004	S1	-0.0552	3136.04
0.25	M1-12	20	2.014919	0.00068	S2	4.01299	
	M1-13	40	4.012995	0.00135	ε2	0.00135	
	M1-21	10	0.986991	0.00027	S1	-0.0233	4418.70
0.50	M1-22	20	1.948994	0.00052	S2	3.9679	
	M1-23	40	3.967901	0.00095	ε2	0.00095	
	M1-31	10	0.825952	0.00026	S1	-0.0568	4084.33
0.75	M1-32	20	1.713276	0.00051	S2	3.45653	
	M1-33	40	3.456527	0.00091	ε2	0.00091	
	M1-41	10	0.843389	0.00032	S1	-0.0582	3258.47
1.00	M1-42	20	1.634291	0.00058	S2	3.30286	
	M1-43	40	3.302863	0.00108	ε2	0.00108	
	M1-51	10	0.917634	0.00026	S1	0.05285	4008.44
1.25	M1-52	20	1.791492	0.00049	S2	3.53239	
	M1-53	40	3.532391	0.00092	ε2	0.00092	
Group 2 (-5^{0}C)							
Steel Fiber (%)	Specimen No.	% Load	Average Stress (ksi)	Average Strain (in/in)	Parameters		Average MOE (ksi)
	M2-11	10	0.83159	0.00036	S1	-0.1634	3205.71
0.25	M2-12	20	1.7926	0.00066	S2	3.47423	
	M2-13	40	3.47423	0.00118	ε2	0.00118	
	M2-21	10	0.75634	0.00028	S1	-0.1045	3615.47
0.5	M2-22	20	1.55534	0.00054	S2	3.07413	
	M2-23	40	3.07413	0.00093	ε2	0.00093	
	M2-31	10	0.92054	0.00032	S1	0.07049	3100.56
0.75	M2-32	20	1.79539	0.00062	S2	3.54282	
	M2-33	40	3.54282	0.00117	ε2	0.00117	
	M2-41	10	0.90849	0.00037	S1	-0.1625	3324.94
1	M2-42	20	1.89467	0.00068	S2	3.71044	
	M2-43	40	3.71044	0.00121	ε2	0.00121	
	M2-51	10	0.9132	0.00036	S1	-0.3124	3758.81
1.25	M2-52	20	1.88153	0.00066	S2	3.78919	
	M2-53	40	3.78919	0.00114	ε2	0.00114	

Group 3 (15^{0}C)							
Steel Fiber (%)	Specimen No.	% Load	Average Stress (ksi)	Average Strain (in/in)	Parameters		Average MOE (ksi)
0.25	M3-11	10	0.74851	0.00022	S1	0.05916	3972.18
	M3-12	20	1.46056	0.00041	S2	2.90405	
	M3-13	40	2.90405	0.00077	ε2	0.00077	
0.5	M3-21	10	0.76163	0.00028	S1	-0.0029	2710.59
	M3-22	20	1.47568	0.0005	S2	2.98881	
	M3-23	40	2.98881	0.00115	ε2	0.00115	
0.75	M3-31	10	0.83074	0.00028	S1	0.00958	3582.20
	M3-32	20	1.71184	0.00053	S2	3.3878	
	M3-33	40	3.3878	0.00099	ε2	0.00099	
1	M3-41	10	0.7037	0.00028	S1	-0.0448	3199.17
	M3-42	20	1.42755	0.00053	S2	2.83154	
	M3-43	40	2.83154	0.00095	ε2	0.00095	
1.25	M3-51	10	0.72791	0.00028	S1	-0.0512	3275.23
	M3-52	20	1.44601	0.00052	S2	2.90866	
	M3-53	40	2.90866	0.00095	ε2	0.00095	
Group 4 (35^{0}C)							
Steel Fiber (%)	Specimen No.	% Load	Average Stress (ksi)	Average Strain (in/in)	Parameters		Average MOE (ksi)
0.25	M4-11	10	0.81655	0.0003	S1	-0.161	3322.37
	M4-12	20	1.6096	0.00056	S2	3.202	
	M4-13	40	3.20184	0.00106	ε2	0.001	
0.5	M4-21	10	0.67195	0.00028	S1	0.123	2461.36
	M4-22	20	1.33214	0.00053	S2	2.664	
	M4-23	40	2.66432	0.00108	ε2	0.001	
0.75	M4-31	10	0.59885	0.00024	S1	-0.034	3229.99
	M4-32	20	1.15556	0.00043	S2	2.266	
	M4-33	40	2.26634	0.00076	ε2	0.001	
1	M4-41	10	0.91194	0.00023	S1	0.048	3534.22
	M4-42	20	1.79288	0.0004	S2	3.545	
	M4-43	40	3.54507	0.00104	ε2	0.001	
1.25	M4-51	10	0.70777	0.00027	S1	-0.161	3383.48
	M4-52	20	1.42818	0.00051	S2	2.867	
	M4-53	40	2.86701	0.00094	ε2	0.001	

Group 5 (55^{0}C)							
Steel Fiber (%)	Specimen No.	% Load	Average Stress (ksi)	Average Strain (in/in)	Parameters		Average MOE (ksi)
0.25	M5-11	10	0.64947	0.00022	S1	0.094	3162.00
	M5-12	20	1.2898	0.00044	S2	2.559	
	M5-13	40	2.55906	0.00083	ε2	0.001	
0.5	M5-21	10	0.5219	0.00015	S1	0.130	3867.69
	M5-22	20	1.02868	0.00029	S2	2.073	
	M5-23	40	2.07262	0.00055	ε2	0.001	
0.75	M5-31	10	0.66685	0.00022	S1	0.148	3014.56
	M5-32	20	1.37734	0.00046	S2	2.724	
	M5-33	40	2.72407	0.0009	ε2	0.001	
1	M5-41	10	0.66778	0.0002	S1	0.173	3537.10
	M5-42	20	1.33597	0.00036	S2	2.649	
	M5-43	40	2.64856	0.00075	ε2	0.001	
1.25	M5-51	10	0.76874	0.00029	S1	-0.030	3162.08
	M5-52	20	1.55803	0.00058	S2	3.123	
	M5-53	40	3.12337	0.00105	ε2	0.001	